# Combustion in Porous Media

**Massoud Kaviany and Mahmood Fatehi**[1]

Detailed description of transport and reaction in inert and combustible porous media requires examinations of: the ratio of the reaction zone thickness to the pore (or particle) size, the extent of thermal nonequilibrium between the solid and gaseous phases, the gaseous and solid phase chemical kinetics, and the extent of solid-gas and solid-liquid phase changes. Here we first examine the fundamentals of transport phenomena in porous media, and then present an overview of much of the work related to the phenomena of combustion in porous media and the applications under which it is important. We discuss some of the pending questions in combustion in inert and combustible porous media and also present our new results on the burning front propagation rate and the degree of solid consumption in reverse combustion. The need for the pore-level examination, for accurate predictions, is addressed.

## INTRODUCTION

When an exothermic reaction releases a sufficient amount of heat, a chemical reaction can be sustained in porous media. Because of the rather large total (combined molecular, dispersive, and radiative) effective thermal conductivity, the peak reaction temperature needed for sustained reaction is lower in porous media (compared to plain media). The reaction can occur in the gas phase only, as in premixed gaseous combustion in the radiant porous burners, or in both the gaseous and solid phases as in smoldering combustion, incineration, and in combustion synthesis. The concentration or dominance of reaction (a heat source) in one of the phases causes a local thermal (and through the chemical kinetics, a chemical) nonequilibrium. Associated with large pores (or particles) is a large gradient in temperature (and concentration) across a pore (i.e., for large pores the reaction zone is only a few pore sizes thick), and therefore, conventional local volume-averaged treatments cannot accurately describe and predict the transport and reaction and the need arises for some modifications based on detailed pore-level examinations. Figure 1 gives a classification of combustion in porous media. The selection of subdivisions are arbitrary, but reflect the present applications involving combustion in porous media. In the following, the existing treatments of conduction, dispersion, and radiation in porous media are discussed. Combustion in inert and combustible porous media is critically reviewed and the results of our experiment-analysis for gas-solid reactions in reverse combustion are presented.

## TRANSPORT PHENOMENA IN POROUS MEDIA

Figure 2 shows how the investigation into the transport phenomena and reaction, as related to combustion in porous media, is presently approached. The experimental treatments have been mostly around the collection of chemical kinetic data and measurement of the temperature and flame (premixed gas in inert porous media) or front (combustible porous media) speed. The local volume-averaged theoretical treatment is the most common analysis technique used.

1. Department of Mechanical Engineering and Applied Mechanics, The University of Michigan, Ann Arbor, MI 48109, USA.

Scientia Iranica, Vol. 1, No. 1, © Sharif University of Technology, April 1994.

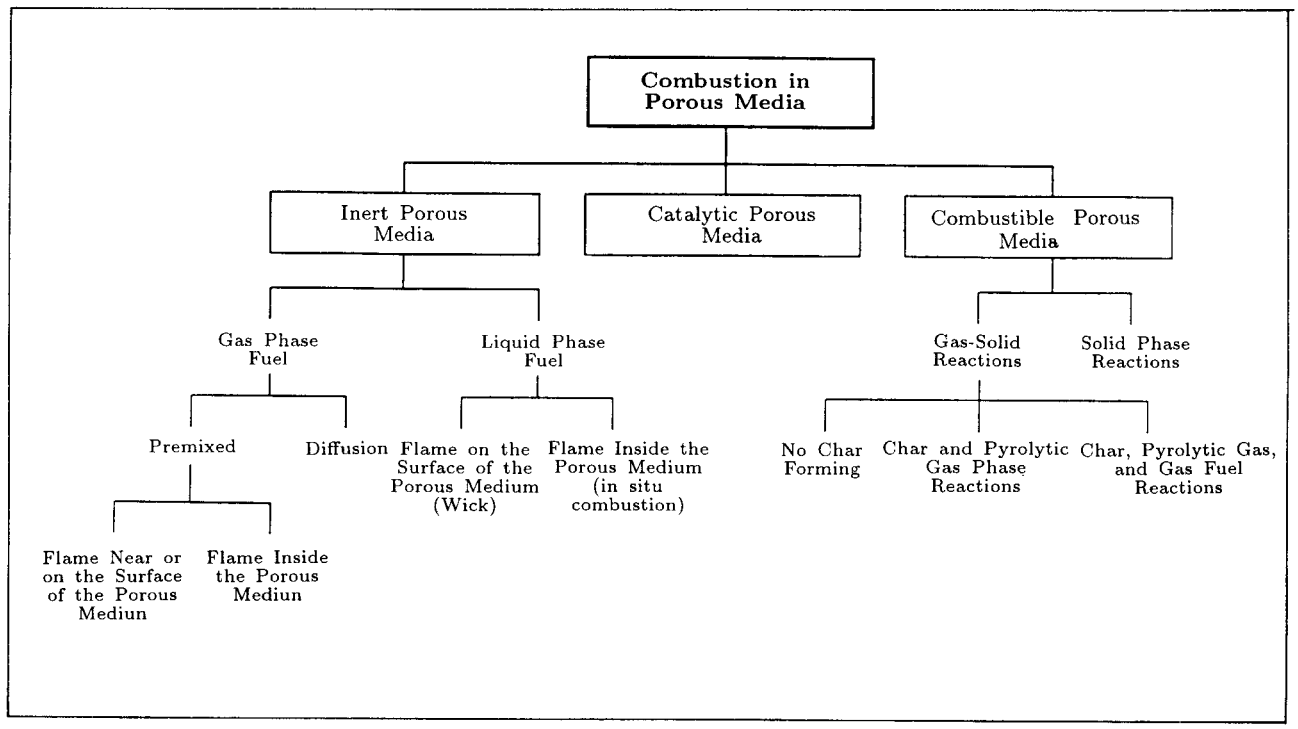


**Figure 1**. A classification of combustion in porous media.

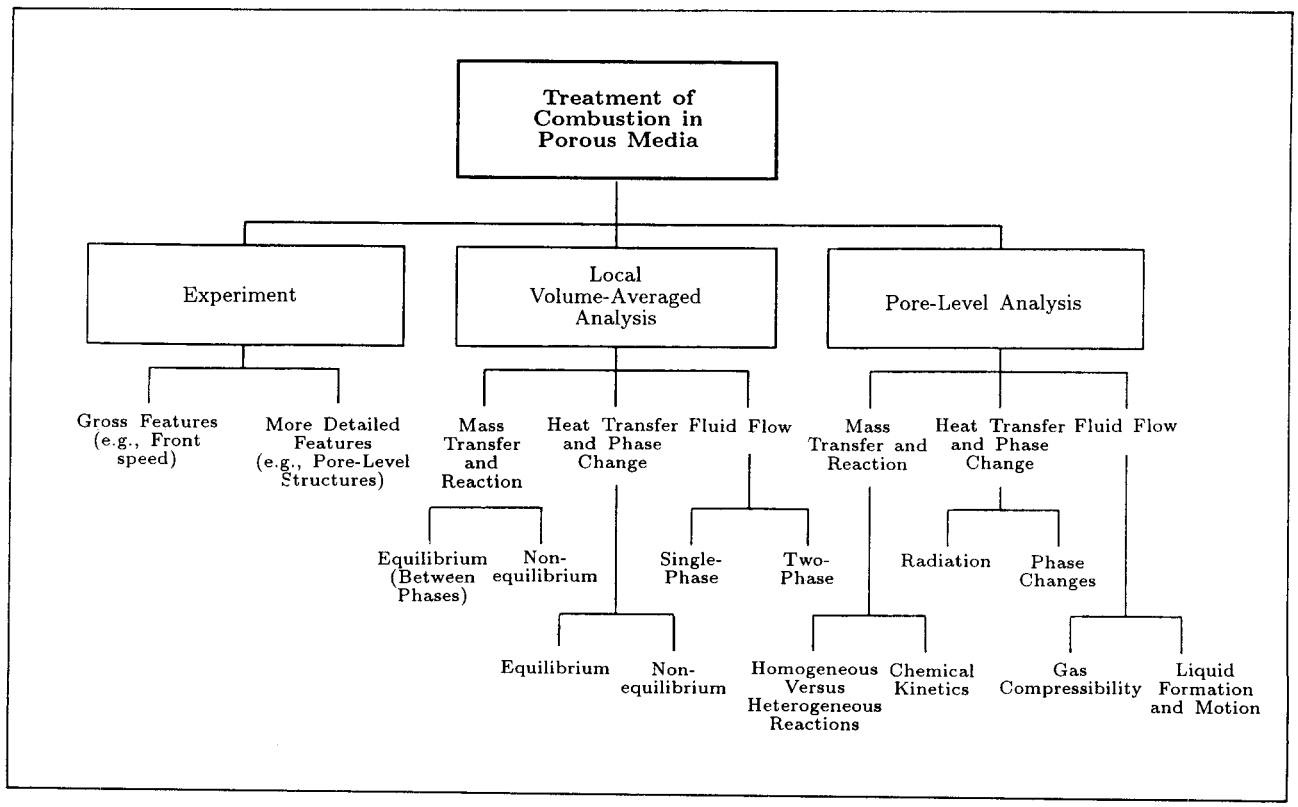


**Figure 2**. Various treatments of transport in porous media as related to combustion.

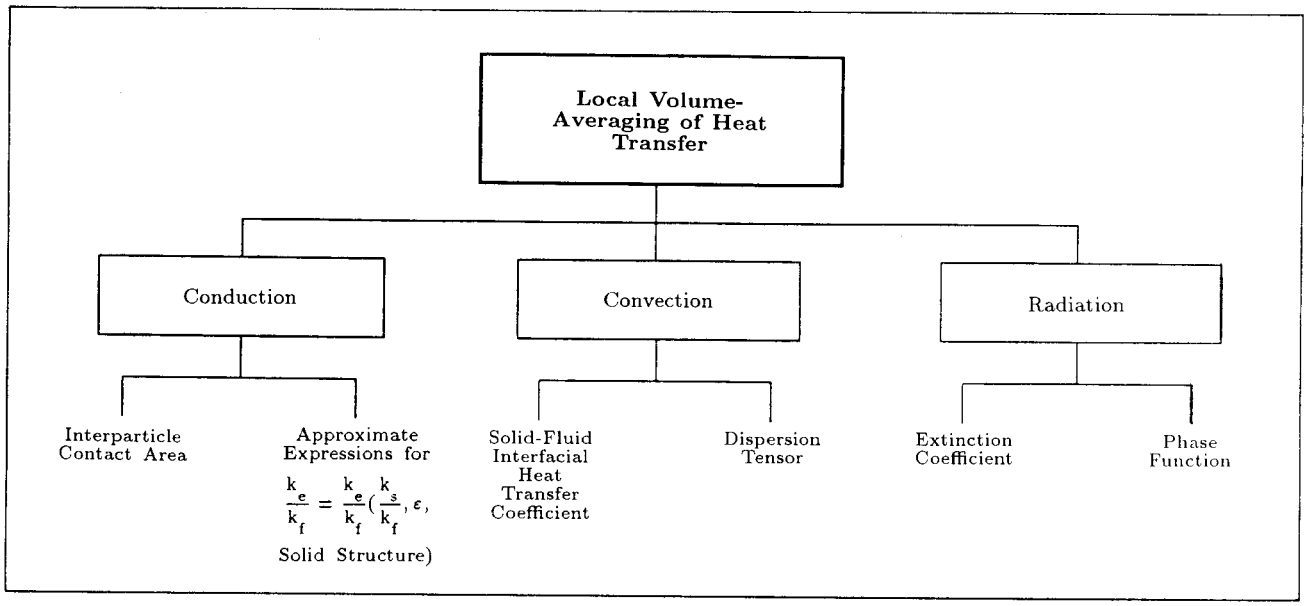


**Figure 3**. Various features of conduction, convection and radiation heat transfer addressed in the local-volume averaged treatments.

Figure 3 shows the various features of conduction, convection and radiation addressed in the local volume-averaged treatments. This technique is generally based on the assumptions of the presence of local thermal equilibrium between the phases and a lack of large volume-averaged gradients in temperature and concentration across the representative elementary volume. Because the heat source is generally dominantly located either in the solid or the fluid phase, the assumption of local thermal equilibrium is not generally valid. Also since the reaction zone can, in some cases, be only a few pore-sizes thick (as in the premixed gaseous combustion in high porosity media), the latter assumption is not always valid.

In the pore-level analysis (which is currently being developed), attempts are made to include all the relevant physical phenomena influencing the transport (including phase change) and reaction. This is done by using rather simple unit cells, but in order to account for the entire reaction zone, many such unit cells must be included in the analysis. Figure 2 shows that in this most detailed analysis, the pore-level heat transfer (including phase change), mass transfer (including reaction) and fluid flow (including two-phase flow and compressibility) are included. Since the use of this method is not practical for general predictive applications, the main objective in using this method is to examine and evaluate the constitutive and coupling coefficients used in the local volume-averaged treatments.

Figure 4 shows the various features of conduction, convection and radiation in porous media. For single-phase flow and heat transfer in packed beds of spherical particles, the bulk (as compared to that near bounding surfaces) effective thermal conductivity tensor $K_e$ has been reviewed [1, 2, 3, 4] and, as is expected when $k_s/k_f$ is much larger than unity, the effect of the consolidation is very significant. The dispersion tensor $D^d$ for randomly packed particles [5] and orderly arranged particles [6, 7] has also been reviewed. The radiative properties have been addressed by Vortmeyer [8] and Singh and Kaviany [9]. The latter reports that even for

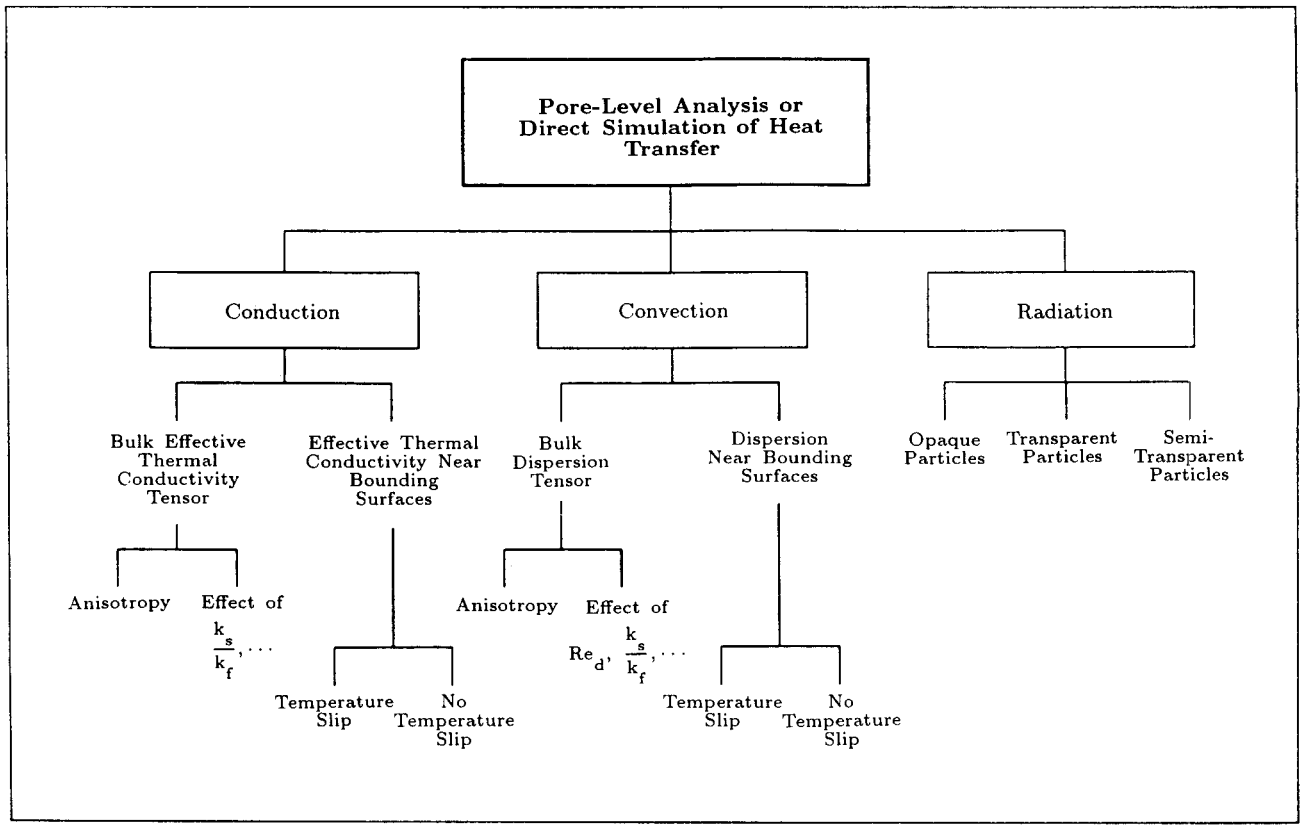


**Figure 4.** Various features of conduction, convection and radiation heat transfer addressed in the pore-level treatments.

porosities as large as 0.9 the radiative interaction among particles is significant whenever the particles are semitransparent or opaque. This is further discussed below.

When no local thermal and chemical equilibrium exists between the phases, various transport couplings occur between the phases. Carbonell and Whitaker [10] present a rigorous analysis of the heat transfer couplings by applying the local volume-averaging technique. Wakao and Kaguei [11] review the earlier simple treatments where a single coupling coefficient is used.

## Radiation

Radiative heat transfer in gaseous packed and fluidized beds can be significant and has attracted considerable interest in the past two decades. The theory of radiative transfer in absorbing, emitting and scattering medium is sufficiently developed and can be found in the standard references [12, 13]. The crucial step in applying this theory to packed beds is in relating the properties of the packed bed to the properties of an individual particle. To do this, the assumption of independent scattering is introduced, i.e., it is assumed that the interaction of the particle with the radiation field is not influenced by the presence of neighboring particles. This condition is satisfied if the spheres behave as point scatterers, i.e., the distance between two particles is large as compared to their size. Also, there must be no interference between scattered fields. The first condition should lead to a limit on the porosity while the second condition would limit the minimum value of $C/\lambda$, where $\lambda$ is the wavelength, $C$ is the average interparticle spacing based on a rhombohedral packing of

spherical particles [$C/d = 0.9047/(1-\epsilon)^{1/3} - 1$] and $d$ is the particle diameter. If both these conditions are satisfied, then the bulk (i.e., away from the bounding surfaces) behavior of the bed can be predicted from the equation of radiative transfer by the theory of independent scattering.

The limits of the theory of independent scattering have been experimentally investigated by Hottel et al. [14]. They identified the limits of independent scattering as $C/\lambda > 0.4$ and $C/d > 0.4$ (i.e., $\epsilon > 0.73$). For a 5% deviation from the independent theory, they recommend $C/\lambda > 0.49$. Brewster [15] also considered larger particles (maximum value of $\alpha_R = 74$). His results indicated that no dependent effects occur as long as $C/\lambda > 0.3$, even for a close pack arrangement ($\epsilon = 0.3$). It was suggested by Brewster [15] that the point scattering assumption is only an artifice necessary in the derivation of the theory and is not crucial to its application or validity. Thereafter, the $C/\lambda$ criterion for the applicability of the theory of independent scattering was verified by Yamada et al. [16] $C/\lambda > 0.5$ for 5% deviation from the independent theory) and by Drolen and Tien [17]. However, Ishimaru and Kuga [18] note dependent effects at much higher values of $C/\lambda$.

In sum, the above experiments seem to have developed confidence in the application of the theory of independent scattering in packed beds consisting of large particles, where $C/\lambda$ almost always has a value much larger than the above-mentioned limit of the theory of independent scattering. Thus the approach of obtaining the radiative properties of the packed beds from the independent properties of an individual particle has been applied to packed beds without any regard to their porosity [15, 17]. However, all the above experiments were similar in design and most of these experiments used suspensions of small, transparent, latex particles. Only in the experiment of Brewster was a close packing of large, semi-transparent spheres considered.

Dependent scattering involves two distinct effects. The first is the far field interference between the scattered waves, which has been studied by Cartigny et al. [19]. They indicate no observable dependent scattering effects for $\alpha_R > 10$, where the size parameter $\alpha_R$ is equal to $\pi d/\lambda$. The far field interference affects only the scattering characteristics of the medium and follows the $C/\lambda$ criterion. The second is the effect of multiple scattering in a representative elementary volume, in which the scattering and absorption characteristics of the particle are affected by the proximity of other particles. This was studied for small (Rayleigh) sized particles by Kumar and Tien [20].

Other researchers have used the Monte Carlo method to predict the radiative heat transfer in packed beds. Yang et al. [21] studied radiative transfer through a bed of randomly packed, specularly scattering spheres. Kudo et al. [22] considered diffusely scattering particles. Tien and Drolen [23] compared the predictions from the various models with existing experimental results [24] and conclude that the independent theory gives a better prediction than the Monte Carlo method. The Monte Carlo method has also been criticized because it cannot treat semi-transparent particles.

The case of absorbing and emitting particles is also reviewed by Tien and Drolen [23] and by Vortmeyer [8]. However the theory of independent scattering fails to satisfactorily explain the experimental results for this very important case. Most notably, the independent theory cannot explain the effect of particle emissivity on the radiative heat transfer.

Singh and Kaviany [9] consider radiative transfer in packed beds of large (geometric range) size particles by using the Monte Carlo method. The far field interference effects which follow the $C/\lambda$ criterion are negligible because particles with very large $d$ will almost always have a high value of $C$. The Monte Carlo technique is extended to accommodate emitting particles as well as semi-transparent particles. Also, the Monte Carlo simulations over a range of porosities are compared to the results obtained from

the equation of radiative transfer and the deviation from the independent theory is shown for smaller porosities. Thus, dependent scattering and absorption are shown to exist even for infinitely large particles, which should fall into the independent range according to the $C/\lambda$ criterion.

Radiation in a medium of cylindrical particles has been studied by various researchers for a medium of high porosity [23, 25, 26]. The existing treatment assumes that the scattering is independent and that the radiative behavior of a particle is not affected by neighboring particles. The single particle properties are calculated from the theory of Mie scattering and the radiative properties of the bed are obtained by the volume averaging on the basis of the theory of independent scattering. This approach is limited by the range of applicability of the theory of independent scattering. The independent theory fails when the ratio of interparticle distance to the particle size is small [23], and when the porosity is small [27].

Although estimates of the limits of independent scattering are available for spheres, extrapolation to cylinders is possible only if a rough estimate is required. An array of cylinders in a typical combustion application will definitely have a lower porosity than the independent limit ($\epsilon \approx 0.95$). The first condition mentioned above, however, will generally be satisfied for wavelengths in the range encountered in combustion applications. One way to solve this problem is to carry out a Monte Carlo simulation. However, apart from requiring a large amount of computing time, it is also not very convenient to use in the presence of other modes of heat transfer.

It is still possible to preserve the continuum treatment if the radiative properties are scaled as a function of the porosity and the method of solution is modified to account for transmission through semi-transparent particles [27]. This treatment is based on separately accounting for the two dependent scattering effects noted in [9], i.e., multiple scattering in a unit volume and the transportation of radiation through a particle across a substantial optical thickness. Multiple scattering, which depends on the porosity alone, is accounted for by scaling the optical thickness. The transmission through the semi-transparent particles is modelled by allowing for the transportation effect while describing the intensity field by the method of discrete ordinates. This is done by taking into consideration the spatial difference between the point where a ray first interacts with a sphere and the point from which it finally leaves the particle. This spatial difference corresponds to an optical thickness (for a given porosity) across which the ray is transported while undergoing scattering.

In order to summarize the above discussion on radiation heat transfer in porous media, we consider a comparison between an available experimental study (this is the most referred to experiment in the literature) and the available predictions. In the experiment of Chen and Churchill [24] an open-ended tubular furnace behaving as a high temperature, black-body source was incident on one surface of a packed bed of spheres. The flux was modulated to a square wave by a mechanical chopper and the intensity of the transmitted radiation was measured with a thermopile detector. The packed bed was designed to simulate a one-dimensional bed by using an aluminum tube with highly reflecting walls as the container. The transmission through the bed was measured using isothermalbeds of glass, aluminum oxide, steel and silicon carbide particles of different shapes.

Figure 5 shows the comparison between the results obtained by Singh and Kaviany [9,27,28] using the Monte Carlo method, those from the independent theory (using the method of discrete ordinates) and that of the Chen and Churchill experiment on steel spheres ($d$=4.76 mm, $T$=1366 K, where $T$ is the temperature of the blackbody source). The spheres are assumed to be specularly reflecting with an emissivity $\epsilon_r$ of 0.4 (as suggested by Chen and Churchill).

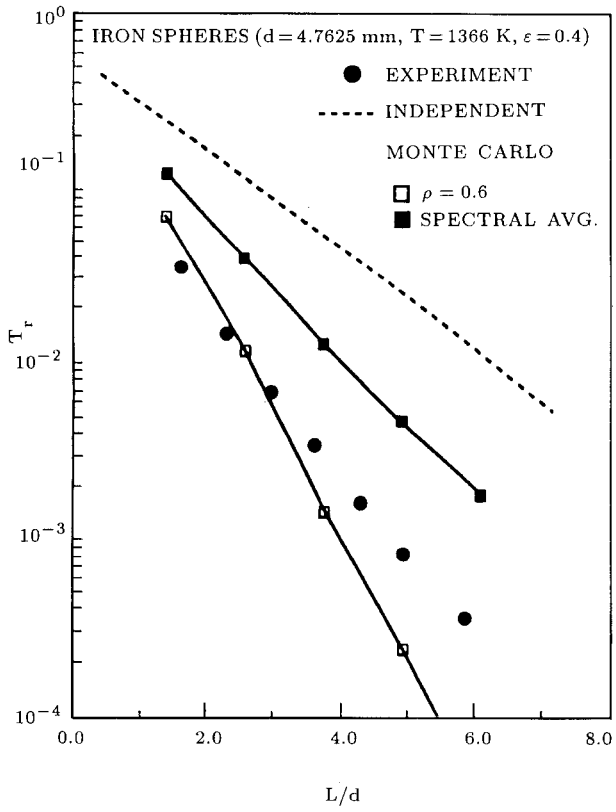


**Figure 5.** Transmittance through a bed of steel spheres. Comparison between the Chen and Churchill experiment and the theoretical predictions.

It can be seen that the independent theory predicts a much higher transmittance than the experimental results of Chen and Churchill. The emissivity can also be calculated theoretically by using the Mie theory or the large size parameter asymptote. The spectrum was divided into five wavelength bands and the wavelengths in the middle of the band were used to calculate the emissivities of a large particle. The optical properties of steel and some other materials are given in Kaviany [4]. Emissivity values ranging from 0.05 to 0.30 were obtained. This would result in a further worsening of the prediction by the independent theory. The Monte Carlo method was used with a randomly packed bed ($\epsilon = 0.58$) generated using the sphere settling program of Jodrey and Tory [29]. Figure 5 shows the Monte Carlo method for the specularly scattering particles for $\epsilon_r = 0.4$, and for a spectrally averaged transmittance. It is clear from the figure that the results from the Monte Carlo method lie in the same range as the experiment. The uncertainty in the emissivity of steel is because of its dependence on the temperature and also due to the presence of an oxide coating as pointed out by Chen and Churchill [24]. It must be stressed that the independent theory fails to explain the experimental results even when a very large allowance is made for the uncertainty in the emissivity. A direct Monte Carlo simulation or a modified continuum method based on the scaling of the radiative properties [28] provides the only successful method to deal with radiation problems in large particle beds.

## COMBUSTION IN INERT AND CATALYTIC POROUS MEDIA

Over the last decade, the advantageous features of combustion in porous media, such as its burning of very lean mixtures, increased combustion efficiency (i.e., shorter combustors are needed), reduced pollutant emission and enhancement in heat removal (e.g., radiation from the solid matrix), have resulted in significant interest in the U. S. and Japan [30-40]. These existing experimental and analytical treatments have revealed some of the gross features of the combustion of premixed gases in porous media. These features include the flame speed and temperature, its approximate location and the existence of multiple and stable flame locations [41]. The combustion in porous media is different from that in the plain media, mostly due to the influence of the solid matrix thermal conductivity and its participation (and dominance) in radiation. The inter-pore transport is drastically influenced due to the no-slip and impermeable conditions at the surface of the solid matrix. The extra longitudinal conductive and radiative heat transfer result in a lower flame temperature, a gross feature that has been widely recognized. However, the role of

the inter-pore diffusion-convection (species) and diffusion-convection-radiation (energy) on the pore-level chemical reactions has not yet been examined. Also not yet attended is the possibility of the existence of surface catalytic reactions (note that most solid matrices are made of ceramics which are composed of many trace elements and these matrices have large specific surface areas).

The multiplicity of the stable flame location and the other features of combustion in porous media is, in principle, similar to that found for flames in refractory tubes [42, 43]. Combustion in refractory tubes, where the flow is generally turbulent, has many features in common with combustion in other porous media which may be made of consolidated or non-consolidated particles. Generally, in porous media made of particles, the Reynolds number based on the particle size is in the laminar regime, but the lateral (as well as longitudinal) thermal and mass dispersion phenomena, similar to the thermal and mass eddy diffusivity in the turbulent flow through tubes, exist due to the simultaneous presence of the velocity and temperature (concentration) gradients in the pore [6,44]. Therefore, compared to the capillary tube flow, the theoretical study of combustion in porous media made of particles can be made more rigorous because the pore-level fluid flow is generally laminar and steady.

In the following, we examine the existing knowledge-base in (a) the area of experiments and measurements on combustion in porous media, (b) the role in combustion and the analyses of radiation in porous media and (c) the local volume-averaged based analyses of flame in porous media. We also point out the lack of a comprehensive treatment in each of these areas which has resulted in inconclusive results on the effects of the solid matrix on the combustion characteristics such as the pollutant emission, the flame temperature and the combustion efficiency.

## Experiments on Combustion

Kotani and Takeno [30] use a porous medium which is a bundle of ceramic capillary tubes (ID of 0.60 and OD of 1.0 mm) with the gas flowing through these tubes. Their methane-air flame is stabilized in these 30 mm long tubes or upstream or downstream from them, depending on the flow rates and the equivalence ratio $\Phi$. Their stability diagram shows that the flame is stable and present downstream of the porous medium for a wider range of flow rates (i.e., range of flame speeds) and equivalence ratios. In the experiment of Echigo et al. [31] an equivalence ratio of 0.1 is used to burn natural gas inside a solid matrix made of sintered, metallic spherical particles. This equivalence ratio is much below the flammability limit for the natural gas and air [45] in plain media. In addition to the burning of the lean gaseous fuel and having a rather short porous combustor, they exploited the radiative heat transfer from the solid matrix to a cooled coil placed downstream from it. In this and the other work from the same group, the emphasis has been on the burning of lean fuels and the radiation heat transfer from the matrix to a downstream, cooled surface.

In contrast to the Japanese research, the U. S. research has emphasized the low pollutant emission aspect of the combustion in porous media [46]. The measurements of Khinkis et al. [34] show that, for some equivalence ratios, the CO production is reduced for flames in porous media, but the measured $NO_x$ has a large scatter and, because of the uncertainty in the measurements, no conclusions can be made about the reduction of $NO_x$ production in porous media. Recent results obtained under the sponsorship of the Gas Research Institute show a definite $NO_x$ reduction (private communication, 1990). In the measurements of Sathe et al. [47], the temperature distribution in the solid phase of a 12.6 cm diameter, 5 cm long cylindrical porous medium (the matrix has cellular structure and is made of 97% alumina-silicate with a porosity

$\epsilon$ of 0.85) is measured. In order to prevent any permanent damage to the ceramic solid matrix, the equivalence ratio $\Phi$ is kept below 0.6. The range of $\Phi$ used is between 0.5 and 0.6. It is not clear if $\Phi < 0.5$ was flammable in their solid matrix, or that it just was not considered. From the measured temperature distribution, the flame (methane-air) location is determined, but they do not find a multiplicity of the flame location. Their predictions of the temperature field (using ad-hoc, local volume-averaged conservation equations) is not in good agreement with the measurements. This is partly due to the scatter in the measurement and partly due to the inadequacy of the local volume-averaged equations. As with the work of Echigo et al., they also measure the radiant heat transfer rate from the solid matrix to a cooled collector. No CO or $NO_x$ measurements have been reported. The solid matrix used has about 4 pores per 1 cm and, with $\epsilon = 0.85$, the average linear pore size is approximately 2 mm. The flame thickness for hydrocarbon-air systems is less than a millimeter [48]. We expect a thickening of the flame with an increase in the axial conduction and radiation heat transfer. We note that this increase is not yet quantified, but it is not expected to be very large. Therefore, the volume-averaged equations are not expected to be applicable. Also, the measurements of the solid-phase (as well as the gas-phase) temperature in the vicinity of the flame requires special spatial resolution. For this reason, the use of a more regular solid matrix structure, such as a bed of spherical or cylindrical particles, is more appropriate if comparison with the predictions is needed. This is especially crucial when examining the lack or the presence of the local thermal equilibrium between the solid and fluid phases.

In the experiments of Khinkis et al. and that of O'Sullivan and Khinkis, ceramic, spherical particles (non-consolidated) are used with the bed of these particles either cooled by the passage of water carrying tubes, or not cooled. For the case of the not internally cooled bed, the flame (natural gas-air) location is very sensitive to the flow rate (i.e., the flame speed is very sensitive to the flame location) and, therefore, a steady flame is found to be difficult to maintain. This results in undesirable flash-back. Their design does not allow for a significant heat loss from the flame when the flame moves upstream. This heat loss is required for the stabilization of the flame. Also, the use of a smaller particle size and a lower porosity upstream of the desired flame location can lead to an increase in the axial conduction heat transfer. Also, if the particles are small enough, the flame may extinguish. The effect of the particle size on the flame extinction has not yet been studied.

### Analyses of Flame Speed and Structure

The one-dimensional analysis of the flame structure in porous media, including the effect of radiation, has been performed by [32, 33, 35, 36, 37, 39]. These analyses are based on a single-medium [32], or a two-medium [33, 35] treatment of the energy conservation. The latter assumes no local thermal equilibrium between the phases and requires the specification of the interstitial area and heat transfer coefficient. The species conservation equations used are some ad-hoc, local volume-averaged equations based on the complete mixing of species within the pores. The thermal and mass dispersions are not included in these volume-averaged equations. This generally leads to large errors, especially when the particle-based Peclet number is larger than unity [11]. The radiation treatment is through a continuum model with the radiation properties either treated parametrically [32, 33] or determined from the independent scattering theory [35]. The existing analyses of the flame structure give the temperature distribution within the porous medium (including the flame location and thickness) and, depending on the chemical reactions included in the prescribed reaction equations, they obtain the concentra-

tion of the products included in the prescription. No $NO_x$ production has yet been modeled. They show that the flame thickness decreases with the decrease in the equivalence ratio (as expected from the flames in plain media), but the expected increase in the flame thickness (additional conduction and radiation heat losses) with the decrease in the porosity (porosity of unity corresponds to the plain media) has not yet been quantified. However, we expect that for high porosity media [32, 35] the flame thickness is about the same or smaller than the linear pore size. Under this condition, the local volume-averaging, which is based on the existence of a representative elementary volume over which the variations of temperature and concentration are small compared to those occuring over the linear dimension of the porous medium, will not hold [10]. Therefore, the available results can only be considered as tentative. For the prediction of the production of the pollutants, which are generally small in concentration, these existing models are not expected to result in accurate predictions.

Examination of the conservation equations presently being used shows that some of the anticipated significant physical phenomena are not included in these equations. In the following, we briefly discuss these phenomena.

### *Momentum Equation*

Although not important for high porosity media, the Darcy resistance in a randomly packed bed of spheres (porosity near 0.4) can be significant. In addition, due to the significant rise in the temperature of the gas, the buoyancy effect becomes very significant. The existing analyses do not include a momentum equation and, therefore, fail to allow for the variation in the pressure which, depending on the orientation of the flow with respect to gravity, the porosity and the particle size, can be very significant (some of the porous media considered for commercial heating applications fall into this category). Since the gas expands very rapidly over length scales of the order of the pore size, in using a local volume-averaged momentum equation, a special treatment is required

### *Energy Equation*

Present models (single- and two-medium treatments) treat the radiation heat transfer using continuum treatments which are based on the volume-averaging of the independent scattering. They also implicitly assume that each particle is isothermal (because the representative elementary volume must contain many particles). Since the flame thickness is of the order of the particle size, the temperature variation across the particles in and around the flame becomes rather large and these existing continuum treatments are not expected to be valid. The thermal dispersion (which is treated as an added diffusion) which is presently neglected, plays a significant role on the temperature distribution. The predicted temperature distribution of Sathe et al. [47] contains a large gradient downstream of the flame, while the experimental results do not show such a trend. This can be due to the neglected thermal dispersion. The existing treatments of the interstitial heat transfer coefficient are not consistent with the rigorous two-medium treatments and must be re-examined [10].

### *Species Equation*

The present treatments neglect the species dispersion. For the case of the mass Peclet numbers larger than unity, this cannot be justified. The particle-based mass Peclet number is defined as $Pe_m = u_D d/D_m$, where $u_D$ is the Darcean velocity, $d$ is the average particle size, and $D_m$ is the molecular mass diffusivity. We note that $Pe_m$ is larger than unity for most applications. One of the most questionable assumptions in the existing treatments is that of the well-mixed pore. In this assumption the production rate of species $i$ is given in terms of the local densities and the local temperature. These densities are

the volume-averaged densities and the assumption is that within a pore the species are well mixed and are available for reaction (i.e., no diffusion control in the pores). The same assumption is made about the temperature. Considering that the flame thickness is of the order of the pore size, significant variations in the concentration and temperature (as well as velocity) across a pore are expected. Therefore, the presence of the solid phase is expected to influence the concentration distributions and, therefore, the reaction rates can be smaller than those predicted using the well-mixed cell models. However, the well-mixed temperature assumption tends to underestimate the reaction rates. The net effect of the variation in densities and temperature determines the actual pore averaged reaction rates. The flame speed as well as the pollutant formation are expected to be dependent on this pore-level diffusion-convection-reaction.

For impermeable particles both homogeneous reactions [49], and heterogeneous reactions [50, 51, 52] can occur. Modeling of the heterogeneous reactions is addressed by Marteney and Kesten [53], Harrison and Ernst [54], Bruno et al. [55], and Fakheri and Buckius [56]. We expect that due to the no-slip boundary condition at the particle surface, the species concentration at the pore-level will be greatly different than the well-mixed assumption of the present ad-hoc treatments.

In summary, although significant progress has been made in the continuum treatments, e.g., the inclusion of the radiation effect and the examination of the presence or the lack of the local thermal equilibrium, the analysis of the flame structure requires a critical, pore-level examination.

## COMBUSTIBLE POROUS MEDIA: GAS-SOLID REACTIONS

The need to predict the propagation speed of the burning front in combustible porous media has resulted in many experimental and modelling efforts. The problem is a subset of the solid phase combustion and has the following peculiarities.

- The amount of oxygen initially present or released during reaction is negligible (oxygen limited).
- Oxygen is sufficient or in excess of the amount needed for complete consumption of the solid (fuel limited).
- The oxygen arrives at the propagation front (and products move away) by travelling through the matrix (burned or unburned region). The burned matrix has a structure (including porosity) that can be substantially different from the original unburned matrix.
- The oxygen supply to the front may be by diffusion, buoyancy motion, forced external surface blowing (cocurrent or countercurrent to the direction of the fuel supply to the front) [57] or forced internal flow (cocurrent or countercurrent).
- The exothermic reactions can be due to oxidation of the volatilized species (gas phase reactions), direct surface oxidization and/or oxidization of char residue produced by prior pyrolysis [58].

The last item, which concerns the reaction mechanisms, is not yet fully investigated and, depending on the temperature of the burning front, one or more of them can occur. We review some of the experimental and modelling efforts in the area of burning of permeable matrices. Our goal is to examine the fluid flow and heat and mass transfer at the pore-level where, at least in the high-porosity matrices, most of the reactions are confined to a region of the order of magnitude of the pore size (i.e., the thickness of the reaction region is of the order of the particle size).

## Experiments on Combustion Wave Propagation

Smoldering (flameless) combustion of permeable matrices [59, 60, 61] occurs in burning of thermal insulation materials (for example, wood-based fibers such as recycled papers), polyurethane foam, cotton, coals, dust, wood dust, etc. [62]. An example of an oxygen supply through buoyant flow (natural convection) is the burning of cellulosic loss fill insulation [63, 64]. Asymptotic propagation speeds of about 0.3 cm/mm (unretanted), which are oxygen-supply controlled, are found. Forced external smolder propagation and transition to flaming in a bed of the same cellulosic insulation material has been studied experimentally by Ohlemiller [65, 66] and Rogers and Ohlemiller [67]. The cocurrent (also called reverse) smolder responds weakly to the increased air velocity $u_a$. The countercurrent (forward) smolder responds strongly and transition to flaming occurs (at $u_a \approx 2\,\mathrm{m/s}$). Forced internal cocurrent smoldering of polyurethane foams has been examined experimentally by Rogers and Ohlemiller [68].

All of the above experiments focus on the oxygen supply to the front, where this supply is assisted by the fluid motion due to buoyancy (where in principle the environment can be normal, micro and zero gravity), or by the imposition of a surface or internal total gas pressure gradient. The compaction of the fuel bed (reduction in porosity $\epsilon$) due to combustion is generally significant in all of these experiments. We view the matrix as being made of consolidated or nonconsolidated particles. In most smoldering experiments, the particle size $d$ is in the range of 50 to 2000 $\mu$m and by using a solely buoyancy-aided smoldering with a front velocity of the order of 100 $\mu$m/min, we arrive at one particle being consumed in roughly 3 to 120 s. An accurate prediction of the rate of the complete combustion of a particle requires further specification of the particle shape and arrangement (microscopic description), bed porosity (a macroscopic description), particle thermophysico-optical properties (including the complex index of refraction), Darcean flow direction (macro) and pore-level flow structure. In oxygen-supply controlled propagation, the front speed would be substantially different in surface-reaction-dominated combustion as compared to the gas-phase-reaction-dominated combustion. This is because of the extra resistance to the flow of oxygen to the particle surface. Also, depending on the thermophysico-optical properties of the solid phase, the heat transfer can, in part, be controlling the propagation rate.

## Analysis of Heterogeneous and Homogeneous Combustion

The existing treatments of the propagation of a burning front in combustible permeable matrices, where both gaseous and solid phase reactions take place, are based on the application of the local volume-averaged conservation equations and the constitutive relations. In some treatments, local thermal and chemical equilibrium are assumed between the solid and the gas phase [62], while other treatments assume local thermal and chemical nonequilibrium [58]. No rigorous examination of the validity of the assumptions of the local thermal and chemical equilibrium are presently available for the problem considered. However, we expect the presence of large temperature and concentration variations around the front, i.e., we expect the reaction region to be of the order of the particle (or pore) size [69]. Therefore, lack of local thermal and chemical equilibrium is expected. In addition, since most of the variations occur over several particle lengths (e.g., diameters), we also expect that the local volume-averaging, (which is based on the presence of smooth variation of the fields over the type of lengths of $O(d)$), will not be applicable. The burning rate for forced internal flow oxidation of fuels has been analyzed by Robinovich and Gurevich [70]. In their analysis, allowance is made for lateral heat losses occur-

ring in a real system, which are responsible for lower front speeds.

We will concentrate on aspects of transport and reaction in the type of porous media that do not undergo significant change in the porosity when the matrix is burned. This is done for the sake of being able to examine in greater detail the thermal and mass transfer control of the burning front speed.

### *Chemical Kinetics*

As was mentioned, the actual chemical kinetics of the solid phase burning of even the simplest solid fuels is rather complicated and is strongly temperature dependent [53]. Ohlemiller [58] gives a thorough review of the gaseous, surface and bulk solid reactions. The solid endothermic reaction leads to the pyrolytic formation of a char and the endothermic sublimation leads to the release of volatiles in the gaseous phase. Therefore, in addition to the direct attack of the oxygen on the solid surface, depending on the temperature, both the gas-phase and the char oxidation must be addressed. A simplified kinetic model that is applicable at the low temperatures is suggested by Ohlemiller et al. [69] for polyurethane foams and allows for the char formation and char oxidation. They give

$$1g(\text{fuel}) + n_{o1}O_2 \rightarrow n_{c1}(\text{char 1}) + (1 + n_{o1} - n_{c1})(\text{gaseous products 1}), \quad (1)$$

$$1g(\text{char 1}) + n_{o2}O_2 \rightarrow n_{c2}(\text{char 2}) + (1 + n_{o2} - n_{c2})\ (\text{gaseous products 2}), \quad (2)$$

where $n_s$ is the stoichiometric coefficients (grams/gram). Dosanjh et al. [62] allow for an endothermic pyrolytic char formation followed by a char oxidation. They suggest that, since the pyrolysis is much faster than the char oxidation, a simple one-step reaction of the form given below be used to model the reaction.

$$1g(\text{unburned solid}) + n_oO_2 \rightarrow n_a(\text{ash}) + n_{gp}(\text{gaseous products}) + \Delta i_c n_o, \quad (3)$$

For cellulosic material, the thermal degradation is modelled by the three global reactions [68] given below.

*Endothermic Pyrolysis*:

$$1g(\text{fuel}) \rightarrow n_{c1}(\text{char}) + (1 - n_{c1})(\text{gaseous products 1}), \quad (4)$$

*Exothermic Thermal Oxidation*:

$$1g(\text{fuel}) + n_{o2}O_2 \rightarrow n_{c2}(\text{char}) + (1 + n_{o2} - n_{c2})(\text{gaseous products 2}), \quad (5)$$

*Exothermic Char Oxidation*:

$$1g(\text{char}) + n_{o3}O_2 \rightarrow n_{a3}(\text{ash}) + (1 + n_{o3} - n_{a3})(\text{gaseous products 3}). \quad (6)$$

Note that the models of Ohlemiller et al. [69] for chemical kinetics and its modifications are phenomenological mixture (gas-solid phase averaged) models and, therefore, do not directly address the solid surface reactions.

Kashiwagi and Nambu [71] determined the first order global kinetic constants for the three-step reaction mechanism for cellulosic paper, Equations 4-6, using thermogravimetry technique. The parameters obtained in their study are listed in Table 1. Rogers and Ohlemiller [68] also report the kinetic constants of $(163\frac{\text{kJ}}{\text{mol}})$ for the activation energy and $6.7 \times 10^8(s^{-1})$ for the pre-exponential factor. Despite the close agreement between the activation energies, the discrepancy between the pre-exponential factors is attributed to the difference between the order or reaction reported by the two sources.

**Table 1.** Global Kinetic Constants

| | Pyrolysis Reaction | Oxidative Degradation Reaction | Char Oxidation Reaction |
|---|---|---|---|
| E (kJ/mol) | 220 | 160 | 160 |
| A ($s^{-1}$) | $2 \times 10^{17}$ | $2.5 \times 10^{12}$ | $5.67 \times 10^{9}$ |

Data from [71].

The kinetic data reported by Roberts [72] indicates two activation energies of 235 and 126($\frac{kJ}{mol}$) for the pyrolysis of wood. He suggests that pyrolysis may take place by either of these kinetics or by a combination of them. Shafizadeh [73] presents two alternative pathways for decomposition of cellulosic materials as

$$cellulose \begin{array}{l} \longrightarrow volatiles, K_v \\ \longrightarrow char + gases, K_c. \end{array} \quad (7)$$

The kinetic rates for cellulose pyrolysis as reported by Shafizadeh are

$$K_v = 3.2 \times 10^{14} exp(-198/RT),$$
$$K_c = 1.3 \times 10^{10} exp(-151/RT)(s^{-1}).$$

Shafizadeh [73] also reports the yields, elemental composition and empirical formulae of chars obtained by isothermal heating of cellulose, wood and lignin samples for 5 min within the temperature range of 300 – 500°C. His results are shown in Table 2. It appears that the chemical composition of the remaining char ($C_6H_{4.5}O_{1.4}$) does not change with the type of the starting material. Since the primary elements that compose wood are cellulose and lignin [74], the illustration presented by Shafizadeh can be extended to include the third reaction (char oxidation with the kinetics data of Kashiwagi and Nambu [71]) to give

$$cellulose \begin{array}{l} \longrightarrow \text{volatiles} \\ \longrightarrow \text{char}_1 + \text{gases}_1 \longrightarrow \text{char}_2 + \text{gases}_2. \end{array} \quad (8)$$

Figure 6 shows some of the features of gas-solid reactions as related to combustion synthesis.

### *Transport Phenomena*

The conservation of mass (overall and species), momentum and energy are presently treated using the local volume-averaged equations along with local equilibrium or a nonequilibrium assumption.

The transient species conservation equations for chemical nonequilibrium between the solid and gas phases must include a total effective mass diffusion tensor $\langle D_m \rangle^g = \langle D_{me} \rangle^g + \langle D_m^d \rangle^g$ where $D_{me}$ is the effective mass diffusivity tensor for the gas phase and $D_m^d$ is the dispersion tensor. When a significant mass diffusion can occur within the solid phase, an allowance has to be made for the effective mass diffusivity of the solid phase. In addition, the mass transfer coefficient $h_m^{sg}$ for the solid-gas interface must be specified. This coefficient is critical in the surface reaction dominated smoldering, and its magnitude determines the extent of the mass transfer control of the front speed. For packed beds of spheres [11] and for consolidated fibrous porous media [75] the heat transfer counterpart of this coefficient is known. However, because of the presence of radiation heat transfer and also since the solid phase allows for thermal diffusion within it, while generally being impermeable, the heat and mass transfer analogy does not hold at the particle level. Therefore, $h_m^{sg}$, which is a significant parameter, is not generally known [58]. Then, the local equilibrium treatments $h_m^{sg} \rightarrow \infty$ [62] are assumed as an alternation. The functional form of $h_m^{sg}$ is

$h_m^{sg} = h_m^{sg}(Pe_d, Sc,$ matrix structure, reaction distribution in solid and gas phases).

In the thermal nonequilibrium treatment of the energy conservation where the temperature of the solid is taken to be different from that of the gas, an interfacial heat transfer coef-

**Table 2.** Starting Material and Elemental Composition of Its Char

| Material | Temperature (°C) | Char Yield (wt%) | Composition C | H | O | Empirical Formula |
|---|---|---|---|---|---|---|
| Cellulose | no treatment | – | 42.8 | 6.5 | 50.7 | $C_6H_{11}O_{5.3}$ |
| | 325 | 63.3 | 47.9 | 6.0 | 46.1 | $C_5H_9O_{4.3}$ |
| | 350 | 33.1 | 61.3 | 4.8 | 33.9 | $C_6H_{5.6}O_{2.5}$ |
| | 400 | 16.7 | 73.5 | 4.6 | 21.9 | $C_6H_{4.5}O_{1.3}$ |
| | 450 | 10.5 | 78.8 | 4.3 | 16.9 | $C_6H_{3.9}O_{1.0}$ |
| | 500 | 8.7 | 80.4 | 3.6 | 16.1 | $C_6H_{3.2}O_{0.9}$ |
| Wood | no treatment | – | 46.4 | 6.4 | 47.2 | $C_6H_{9.9}O_{4.6}$ |
| | 400 | 24.9 | 73.2 | 4.6 | 22.2 | $C_6H_{4.5}O_{1.4}$ |
| Lignin | no treatment | – | 64.4 | 5.6 | 24.8 | $C_6H_{6.5}O_{2.0}$ |
| | 400 | 73.3 | 72.7 | 5.0 | 22.3 | $C_6H_{5.0}O_{1.3}$ |

Data from [78]

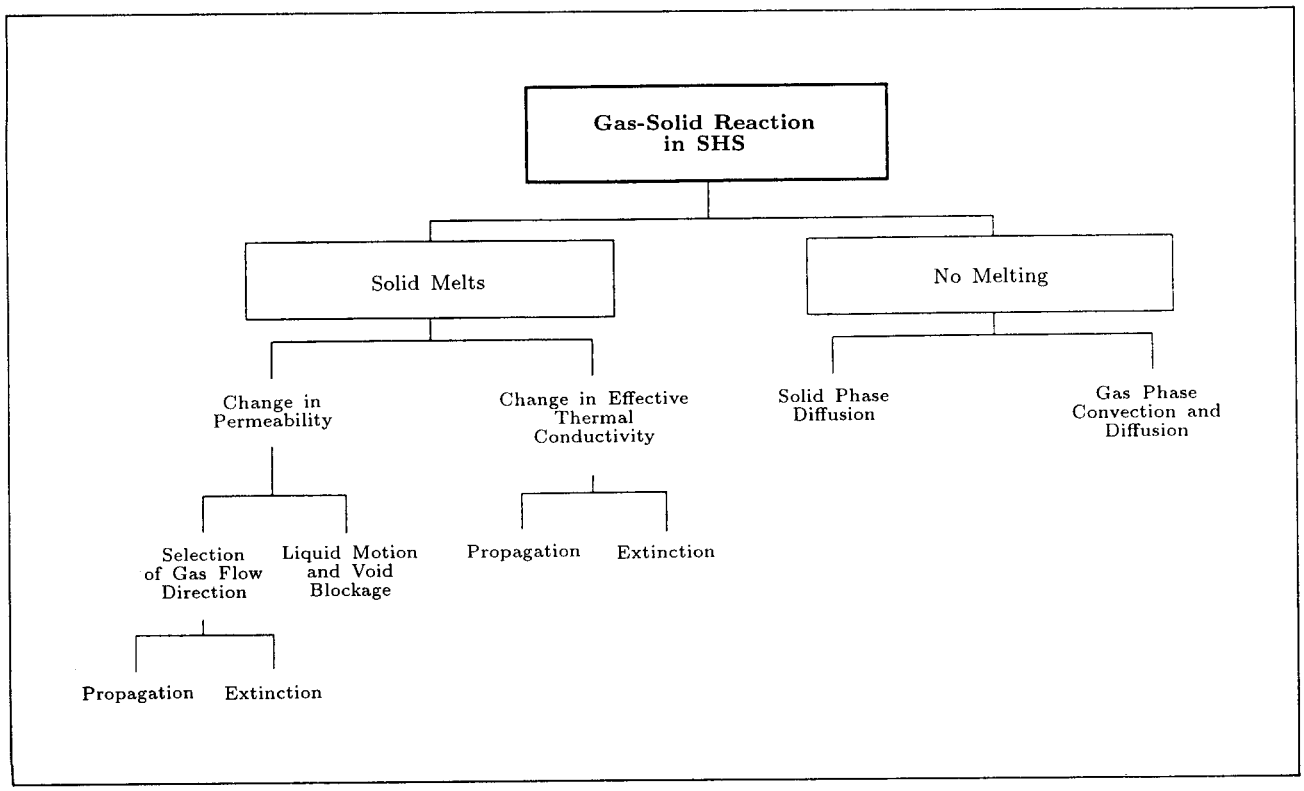


**Figure 6**. Some features of gas-solid reaction in combustion synthesis.

ficient $h^{sf}$ is introduced. A recent measurement of this coefficient for fibrous metallic matrices is given by Golombok et al. [75]. The transient energy equation for the gas phase must include the total effective thermal diffusivity tensor $\langle D\rangle^g = \langle D_e\rangle^g + \langle D^d\rangle^g$ and the interfacial ($s$-$g$) heat transfer coefficient $h^{sg}$. The functional form of $h^{sg}$ is

$h^{sg} = h^{sg}(Pe_d, Pr$, matrix structure, reaction distribution in solid and gas phases, $k_s/k_g)$.

Presently there is no rigorous treatment of $h^{sg}$ for solid and gas phase reactions. Note that $h^{sg}$ depends on both the flow field (which in turn depends on the temperature field) and the temperature field (which in turn depends on the reaction distribution within phases). The radiation heat transfer is generally given as the local volume-averaged radiant heat flux $q_r$ and this local value is based on a significant penetration of the radiation within the bed. For nearly opaque particles, the radiation attenuates in a rather short distance (order of the particle size) and, therefore, the continuum treatment is not expected to be valid.

The transient momentum equation for the phase flow must allow for the inertial, viscous (Darcean) and gravity forces as well as the high velocity effect (Ergunean) and the imposed pressure gradient. Since the gas undergoes significant expansion, the direction of gravity vector with respect to the flow direction becomes important (assisting or opposing the flow). At the pore level, the significant expansion occuring over a distance of the order of the pore size combined with the reaction distributions result in a significant alteration of the velocity field (as compared to the pore-level flow upstream and downstream of the front).

### *Conservation and Constitutive Equations (Reverse Combustion)*

Currently, we have undertaken direct numerical simulation of combustion in inert porous media. The results of such simulations (which shall also include combustible porous media) will be used in modifying the existing volume-averaged equations to account for their limitations. However, until the conclusive results of these numerical simulations at the pore level become available, we will continue to explore the volume averaging approach to find a description for the global characteristics of the combustion process.

In reverse combustion with the burning front propagating parallel to the gas flow, if the thickness of the reaction zone is small compared to the curvature of the wave, combustion can be modelled as a one-dimensional process. The volume-averaged energy equation (with the assumption of local thermal equilibrium between the gas and the solid phase) is written as

$$[\epsilon\rho_g c_{pg} + (1-\epsilon)\rho_s c_s]\frac{\partial T}{\partial t} + (\epsilon\rho_g c_{pg} u_g)\frac{\partial T}{\partial x} = \frac{\partial}{\partial x}[(k_r + k_t)\frac{\partial T}{\partial x}] + (\Delta i_c/n_o)\dot{n}_o. \quad (9)$$

For simplicity, the averaging symbols $<\ >$ are omitted in this section. By defining a new coordinate system that is fixed at the combustion front and travels at a steady rate, $u_f$, with the combustion wave,

$$x_1 = x + u_f t, \quad (10)$$

Equation 9 can be transformed to

$$\frac{d}{dx_1}\{(1-\epsilon)\rho_s c_s u_f T + \epsilon\rho_g c_{pg}(u_g + u_f)T\} = \frac{d}{dx_1}\{(k_r + k_t)\frac{dT}{dx_1}\} + (\Delta i_c/n_o)\dot{n}_o. \quad (11)$$

In the new coordinate system, the volume-averaged conservation equations for the gas and the solid phase, as well as $O_2$ and the unburned solid, are given by

$$\frac{d}{dx_1}\{\epsilon\rho_g(u_g + u_f)\} = \dot{n}_o + \dot{n}_{gp}, \quad (12)$$

$$\frac{d}{dx_1}\{(1-\epsilon)\rho_s u_f\} = \dot{n}_{us} + \dot{n}_a, \tag{13}$$

$$\frac{d}{dx_1}\{\epsilon\rho_g Y_o(u_g + y_f)\} = \frac{d}{dx_1}\{\epsilon\rho_g D_m \frac{dY_o}{dx_1}\} + \dot{n}_o, \tag{14}$$

$$\frac{d}{dx_1}((1-\epsilon)\rho_s Y_{us} u_f) = \dot{n}_{us}. \tag{15}$$

The reaction rate for the consumption of oxygen species is modelled as a one-step, first-order Arrhenius kinetics

$$\dot{n}_o = -An_o\rho_o^a\rho_s^b T^c e^{\frac{-E}{RT}}. \tag{16}$$

Based on the one-step global reaction of Equation 3, the other reaction rates can be written as

$$\dot{n}_{gp} = n_{gp}\dot{n}_o,$$
$$\dot{n}_{us} = \frac{1}{n_o}\dot{n}_o,$$
$$\dot{n}_a = \frac{(1-(n_{gp}-1)n_o)}{n_o}\dot{n}_o. \tag{17}$$

Assuming that the reaction takes place at the solid surface, define $Y_{us}$ as

$$Y_{us} = \frac{\rho_{us}}{\rho_{si}}, \tag{18}$$

such that Equation 16 can be represented as

$$\dot{n}_o = -An_o(\rho_g Y_{os})^a(\rho_{si}Y_{us})^b T^c e^{\frac{-E}{RT}}, \tag{19}$$

where $Y_{os}$ denotes the mass fraction of oxygen at the solid surface. Considering the mass nonequilibrium between the concentration of $O_2$ species in the gas phase (within the pores) and that at the solid surface, the reaction rate can be controlled by the rate at which oxygen can diffuse to the surface of the solid particles. The reaction rate is therefore modified to

$$\dot{n}_o = \frac{1}{\frac{1}{h_D} + \frac{1}{K}}, \tag{20}$$

where

$$h_D = -h_m^{sg}\rho_g \frac{A_{sg}}{V_g}(Y_o - Y_{os});$$
$$Y_o \gg Y_{os}(\text{fast kinetics}), \tag{21}$$

and

$$K = -n_o A(\rho_g Y_o)^a(\rho_{si}Y_{us})^b T^c e^{\frac{-E}{RT}};$$
$$Y_o = Y_{os}. \tag{22}$$

In comparison to $h_D$, the kinetically controlled reaction rate expressed by Equation 22 becomes significant when temperature is low or the size of the solid particle is very small, such that $Y_o = Y_{os}$. Thus, two distinct regimes of reaction can be identified,

$$h_D \gg K \Longrightarrow$$
$$\dot{n}_o = K(\textit{kinetically controlled}), \tag{23}$$

$$h_D \ll K \Longrightarrow$$
$$\dot{n}_o = h_D(\textit{diffusion controlled}). \tag{24}$$

In Equation 21, the ratio of the total surface area of the solid to the volume of the gas is given by

$$\frac{A_{sg}}{V_g} = \frac{6(1-\epsilon)}{\epsilon d}. \tag{25}$$

The interfacial mass transfer coefficient, $h_m^{sg}$ (in analogy with the interfacial heat transfer coefficient), is assumed to be [11]:

$$h_m^{sg} = \frac{ShD_{mg}}{d} = 2 + 1.1Re^{0.6}Sc^{0.33}, \quad (26)$$

where the Reynolds and Schmidt numbers are defined as $Re = \epsilon u_g d/\nu_g$ and $Sc = \nu_g/D_{mg}$ respectively. The balance between the mass fraction of gaseous and solid species are expressed as

$$Y_o + Y_{gp} + Y_I = 1, \quad (27)$$

$$Y_{us} + Y_a = 1. \quad (28)$$

Assuming small pressure variations in the porous medium and across the combustion wave, the conservation equations are solved without considering the momentum equation. With the assumption of constant pressure, the gas density and temperature are related through the equation of state, $P = \rho_g RT$.

The boundary conditions required to solve Equations 11-15 and Equation 20 are given by

*Cold boundary:*

$$x \to -\infty \Rightarrow T = T_u, Y_o = Y_{ou}, Y_{gp} = 0,$$
$$Y_I = 1 - Y_{ou}, Y_{us} = 1, Y_a = 0, u_g = u_{gu}, \quad (29)$$

*Hot boundary:*

$$x \to +\infty \Rightarrow \frac{dT}{dx} = O.,$$
$$Y_o = 0,$$
$$Y_{gp} = 1 - Y_I,$$
$$Y_{us} = Y_{usb},$$
$$Y_a = 1 - Y_{usb} \cdot \text{(oxygen limited)}, \quad (30)$$

$$x \to +\infty \Rightarrow \frac{dT}{dx} = 0.,$$
$$Y_o = Y_{op},$$
$$Y_{gp} = 1 - Y_I - Y_{ob},$$
$$Y_{us} = 0,$$
$$Y_a = 1 \cdot \text{(fuel limited)}. \quad (31)$$

The total effective mass diffusivity $D_m$ in Equation 14 is written as [4]:

$$D_m = D_{me} + D_m^d, \quad (32)$$

where

$$D_{me} = \frac{2\epsilon}{3 - \epsilon} D_{mg}, \quad (33)$$

and $D_{mg}$ is the molecular mass diffusivity which is a function of temperature

$$\frac{D_{mg}}{D_{mg,u}} = \left(\frac{T}{T_u}\right)^{1.75}.$$

The dispersion component, $D_m^d$, is written as

$$D_m^d = D_{mg}\left[\frac{3}{4}Pe_m + \frac{1}{6}\pi^2 (1 - \epsilon)Pe_m lnPe_m\right], \quad (34)$$

and the Peclet number is defined as

$$Pe_m = \frac{\epsilon u_g d}{2D_{mg}}. \quad (35)$$

The total effective thermal conductivity is written as

$$k_t = k_e + \epsilon k_t^d, \quad (36)$$

where

$$k_e = k_g\left[\left(\frac{k_s}{k_g}\right)^{0.280 - 0.757log\epsilon - 0.057log\left(\frac{k_s}{k_g}\right)}\right], \quad (37)$$

and

$$k_t^d = k_g\left[\frac{3}{4}Pe_t + \frac{1}{6}\pi^2(1 - \epsilon)Pe_t lnPe_t\right]. \quad (38)$$

The thermal Peclet number, $Pe_t$ is defined by

$$Pe_t = \frac{\epsilon u_g d}{2\alpha_g}. \quad (39)$$

The radiant heat conductivity is represented as

$$k_r = 4Fd\sigma T^3, \quad (40)$$

where $F$ is the exchange factor (for randomly packed opaque particles, $F = 0.68$ [4], $d$ is particle size, $\sigma$ is the Stefan-Boltzman constant. The total effective conductivity (thermal diffusion and radiation) is then written as

$$k = k_r + k_t. \quad (41)$$

### *Results for Combustion of a Packed Bed of Wood Particles*

Considering a quasi-steady, one-dimensional model for the propagation of the burning front in a porous medium, we solve the volume-averaged conservation equations and the constitutive relations using large activation energy asymptotics. It is of interest to predict the propagation rate of the combustion wave and to determine the peak temperatures attainable in the bed, as well as the extent of conversion of the original material to the products (gas and condensed) and its dependency on the gas flow rate and initial oxygen concentration. The results compare favorably with our experimental results and numerical simulation of the process.

### Large Activation Energy Asymptotics (oxygen limited)

The method of large activation energy has been employed to obtain the burning temperature and the propagation velocity of the combustion front. For the sake of brevity, only the major steps in developing the asymptotic theory have been presented here. It is assumed that

$$\epsilon_0 = \frac{1}{\sigma} = \frac{E}{RT_b} \gg 1,$$

$$A\rho_g = const.,$$

$$\rho_g k_g = const., \text{ and}$$

$$c_{pg} = c_s = c_p = const.$$

The energy equation and the conservation of species for the gas and solid, Equation 11, assuming $a = b = 1$, $c = 0$ in the reaction rate (note that the pre-exponential factor in the reaction rate, A, takes the dimension of $m^3s^{-1}/kg.$) and Equation 14-15, along with the boundary conditions, Equations 29-30, are transformed to

$$\frac{d\tau}{d\xi} = [1 + R_c(1+\phi\tau)^3]\frac{d^2\tau}{d\xi^2} + 3R_cK_t\phi(1+\phi\tau)^2\left(\frac{d\tau}{d\xi}\right)^2 - \Gamma'(1-\tilde{Y})(1-\tilde{Y}_s)e^{\frac{-E}{RT}}, \quad (42)$$

$$\frac{d\tilde{Y}}{d\xi_1} = \frac{1}{Le_g}\frac{d^2\tilde{Y}}{d\xi_1^2} + \Gamma''(1-\tilde{Y})(1-\tilde{Y}_s)e^{\frac{-E}{RT}}, \quad (43)$$

$$\frac{d\tilde{Y}_s}{d\xi_1} = \Gamma'''(1-\tilde{Y})(1-\tilde{Y}_s)e^{\frac{-E}{RT}}, \quad (44)$$

with the boundary conditions

$$\xi \to -\infty : \tau = \frac{d\tau}{d\xi} = 0, \quad (45)$$

$$\xi \to 0 : \tau = 1; \frac{d\tau}{d\xi} = 0, \quad (46)$$

$$\xi_1 \to -\infty : \tilde{Y} = 0; \quad (47)$$

$$\frac{d\tilde{Y}}{d\xi_1} = \tilde{Y}_s = \frac{d\tilde{Y}_s}{d\xi_1} = 0, \quad (48)$$

where

$$\xi = \int \frac{\overline{\rho u} c_p}{k_t} dx_1; \xi_1 = \int \frac{\epsilon \rho_g u_g c_p}{k_g} dx_1, \tag{49}$$

$$\tau = \frac{T - T_u}{T_b - T_u};$$

$$\tilde{Y} = 1 - \frac{Y_o}{Y_u}; \tag{50}$$

$$\tilde{Y}_s = 1 - \frac{Y_{us}}{Y_{us,u}},$$

$$\phi = \frac{T_b - T_u}{T_u}; \tag{51}$$

$$R_c = \frac{4F d\sigma T_u^3}{k_t},$$

$$Le_g = \frac{k_g}{\epsilon \rho_g D_m c_p}, \tag{52}$$

$$\Gamma' = \frac{A_u k_t \rho_{si} n_o}{\epsilon u_{gu} \overline{\rho u} c_p},$$

$$\Gamma'' = \frac{A_u n_o k_{gu} \rho_{si}}{c_p (\epsilon u_{gu})^2 \rho_{gu}}, \tag{53}$$

$$\Gamma''' = \frac{A_u k_{gu} Y_{ou}}{\epsilon u_{gu} c_p u_f (1 - \epsilon)}.$$

In Equation 49, the total mass flux is written as

$$\overline{p} = \rho_s (1 - \epsilon) u_f + \rho_g \epsilon u_g = const., \tag{54}$$

and the following relationship is established between the variables $\xi$ and $\xi_1$

$$\xi = C_1 \xi_1;$$

$$C_1 = \frac{\overline{pu} k_{gu}}{\epsilon \rho_{gu} u_{gu} k_t}. \tag{55}$$

***Outer Solution (convective/diffusion zone):***

In the outer region, reaction is considered to be negligible and the profiles for oxygen and solid species in the outer region have the solution

$$\tilde{Y}^- = C_Y exp(Le \xi_1) = C_Y exp\left(\frac{Le_g}{C_1} \xi\right), \tag{56}$$

where $C_Y$ can be found from matching the inner and outer solutions,

$$\frac{d\tilde{Y}_s^-}{d\xi_1} = 0 \Longrightarrow \tilde{Y}_s^- = const. \tag{57}$$

With zero mass diffusivity for the solid species,

$$\xi_1 \to 0; Y_{us} = 1 \Longrightarrow \tilde{Y}_s^- = 0. \tag{58}$$

Similarly, after determining $\phi$ from the inner solution, the temperature profile in the convective/diffusion zone can be obtained from the energy equation (with no reaction),

$$\frac{d\tau^-}{d\xi} = [1 + R_c (1 + \phi \tau^-)^3] \frac{d^2 \tau^-}{d\xi^2} + 3 R_c K_t \phi (1 + \phi \tau^-)^2 \left(\frac{d\tau^-}{d\xi}\right)^2. \tag{59}$$

***Inner Solution (diffusion/reaction zone):***

Define

$$\delta = \frac{1}{\epsilon_0} = \frac{RT_b}{E} \ll 1, \tag{60}$$

and a new spatial coordinate $\eta$ which is scaled by $\delta$,

$$\eta = \frac{\xi}{\delta}. \tag{61}$$

Since, in the inner region, the temperature can only suffer O ($\delta$) reduction from the leading order, the total thermal conductivity is taken to be

$$k = k_{rb} + k_t;$$
$$k_{rb} = 4Fd\sigma T_b^3, \tag{62}$$

as opposed to $k_t$ in Equation 49. This will simplify the energy equation, Equation 42, in the inner zone by setting $R_c = 0$.

Expand the inner solutions in terms of $\delta$ up to the first leading order as

$$\tilde{Y}^+ = 1 - \delta\gamma(\eta) - O(\delta^2), \tag{63}$$

$$\tau^+ = 1 - \delta\theta(\eta) - O(\delta^2), \tag{64}$$

$$\tilde{Y}_s^+ = \delta\Lambda(\eta) + O(\delta^2). \tag{65}$$

It can be shown that

$$\gamma(\eta) = \frac{Le_g}{C_2^2}\frac{\Gamma''}{\Gamma'}\theta(\eta), \tag{66}$$

and similarly

$$\frac{d\theta(\eta)}{d\eta} = \frac{C_2\Gamma'\delta}{\Gamma'''}(\Lambda - \Lambda_1), \tag{67}$$

where, in the above equation, $\Lambda(\eta = 0) = \Lambda_1$ and $C_2 = C_1\frac{k_t}{k}$. From Equation 60 the following relationships can be defined

$$exp\left(\frac{-E}{RT}\right) = exp\left(\frac{-T_b}{\delta T}\right)$$
$$= exp(-\epsilon_0)exp\left(\frac{-\phi\theta}{1+\phi}\right). \tag{68}$$

Also define

$$\hat{\Theta}(\eta) = \frac{\phi\theta(\eta)}{1+\phi}. \tag{69}$$

The formulation for the inner region is completed by giving

$$\frac{d^2\hat{\Theta}(\eta)}{d\eta^2} = \frac{Le_g\delta^2\Gamma''}{C_2^2}[1 - \frac{\Gamma'''}{C_2\Gamma'}$$
$$- \frac{\Gamma'''}{C_2\Gamma'}\left(\frac{1+\phi}{\phi}\right)\frac{d\hat{\Theta}(\eta)}{d\eta}]$$
$$exp(-\epsilon_0)\hat{\Theta}(\eta)exp(-\hat{\Theta}), \tag{70}$$

$$\eta \to 0 : \hat{\Theta} = \frac{d\hat{\Theta}}{d\eta}|_{\eta=0} = 0, \tag{71}$$

$$\lim_{\eta\to-\infty}\frac{d\hat{\Theta}(\eta)}{d\eta} = -\frac{\phi}{1+\phi}. \tag{72}$$

The condition for the stoichiometry of the reaction is represented by

$$\frac{\Gamma'''}{C_1\Gamma'} = 1 \Longrightarrow n_o u_f(1-\epsilon)\rho_{si}$$
$$= \rho_{gu}u_{gu}\epsilon Y_{ou}. \tag{73}$$

The solution to Equation 70 gives the following expression for the peak temperature in the bed

$$T_b^4 exp\left(\frac{-E}{RT_b}\right) =$$
$$\frac{(E\Delta i_c)^2(\epsilon D_m)(\epsilon\rho_{gu}u_{gu}Y_{ou})^2}{(Rk)^2A_u n_o^3\rho_{si}}. \tag{74}$$

The propagation velocity of the burning front is obtained from Equation 54 and the integrated energy equation given below

$$\Delta i_c = \frac{\bar{\rho}uc_p n_o(T_b - T_u)}{\rho_{gu}u_{gu}\epsilon Y_{ou}}., \tag{75}$$

Relaxing the assumption of equal heat capacities for the solid and air gives the following expression for the adiabatic flame temperature, $T_{ba}$ (corresponding to the stoichiometric burning),

$$T_{ba} = \frac{\Delta i_c Y_{ou}}{c_s\left(Y_{ou} + n_o \frac{c_{pg}}{c_s}\right)} + T_u, \tag{76}$$

and the inlet air velocity for the total consumption of the solid fuel and oxygen can be computed from the following expression,

$$u_{gu,s} = \frac{T_{ba}^2 exp(-E/2RT_{ba})k}{(E/R)\sqrt{\epsilon^3}\Delta i_c Y_{ou}\rho_{gu}}\sqrt{\frac{A_u n_o^3 \rho_{si}}{D_m}}. \tag{77}$$

The rate at which the combustion front propagates under the stoichiometric condition can then be determined from Equation 73 using $u_{gu,s}$ as the incoming air velocity. Note that in the above equation, $D_m$ and $k$ also depend on the incoming air velocity, Equation 32-41, through

$$D_m = D_m(u_{gu}, d, \epsilon, T_{ba}, D_{mg}),$$
$$k = k(u_{gu}, d, \epsilon, T_{ba}, k_s, k_g, \alpha_g),$$

so that the solution for $u_{gu,s}$ should be carried out iteratively.

## Numerical Solution

The governing equations for energy and conservation of species (gas and solid), subject to the boundary conditions, are discretized by integrating the equations over a finite control volume, thus reducing the boundary value problem to a system of algebraic equations. Constant properties are assumed, except for the temperature dependency of the radiative heat transfer coefficient. A nonuniform mesh with a higher concentration of nodal points near the location of the combustion front covers the computational domain. The discretized equations are solved using the power-law scheme [76] to evaluate the fluxes at the control volume faces. The reaction rates, acting as the source or sink terms in the governing equations are linearized according to

$$S = S_c + S_p X_p, \tag{78}$$

where $X_p$ denotes the functional dependency of the source term on the parameter $X$ at location $p$. Since the expression for the reaction rates is quite complex, $S_p$ is taken to be zero and $S_c$ is taken to be constant and equal to the value of the reaction rate at the previous iteration step.

Time-independent profiles are assumed in a coordinate system moving with the combustion front. The species and temperature profiles, as well as the front velocity, are solved iteratively, assuming a uniform gas flux upstream and a constant burning front velocity which depends on the final temperature through the integrated energy equation. Variations of the gas density and the binary mass diffusion coefficient with temperature and evolution of the pyrolytic gas are accounted for. The specific heats and thermal conductivities for air and wood are assumed constant, but can easily be incorporated in the numerical code.

Since the propagation velocity of the combustion front is not known a priori, the location of the front is fixed by specifying the temperature at one mesh point, thus avoiding the cold-boundary difficulty. This point is selected in such a way to insure that the temperature and species gradients nearly vanish at the cold boundary, which otherwise would result in loss of heat through the cold boundary.

An initial profile is assumed for the gas, solid and temperature. The starting profile involves a reaction zone through which the oxidant and solid species concentration change linearly from upstream values to zero. A linear profile is also assumed for the temperature rise in the reaction zone. Zero gradients at the cold and hot boundaries are also imposed on the starting

estimates.

The species profiles are first computed using a fixed temperature. Only after a converged solution is obtained for the gaseous and solid species, with the temperature held fixed, is the energy equation included in the iteration. The energy equation is solved next keeping the concentration of species constant. With the newly converged temperature profile held fixed, the computation on the species equations is repeated. This iterative process is continued until full convergence of all profiles is achieved. The convergence criterion adopted either for the species or the temperature profiles is such that the value for the normalized difference between any two successive computations in the entire computational domain is less than $10^{-9}$. Due to the nature of the reaction rates, as the temperature increases, the source term increases, causing instabilities in the computation of the energy equation. It is necessary to compute the reaction rates only during the iterations on the species equation, and keeping it constant while solving for the energy equation.

## Experiment

Figure 7 shows a schematic of the apparatus used in our experiments. The major component is a fixed bed of fuel which is composed of a random packing of spherical wood particles $6.4 \times 10^{-3}$ (m) in diameter. The particles are placed in a combustion chamber which has a square cross-sectional area and is made of alumina silica (the composition is roughly 80% alumina and 20% silica) to minimize lateral heat losses. A flow dispersion bed containing glass beads is positioned in the lower section of the combustion chamber to insure flow uniformity of the incoming air and minimizing channeling. The fuel is ignited from above by a radiant heat source which provides a uniform ignition of the bed. Subsequent to the ignition of the top layer, the external heat source is removed, and the combustion front starts to propagate at a steady rate. Temperature reading are taken by Pt30% Rh thermocouples (insulated in ceramic tubes) inserted along the centerline of the bed. Measurements are made at the center of the bed to assure nearly one-dimensional behavior and to minimize side effects. The thermocouples are precisely spaced $9.4 \times 10^{-3}$ (m) apart. These provide the propagation velocity and temporal variation of temperature within the bed. Temperature recordings are made in 10 second intervals. The velocity is determined from the known spacing and from the measured time it takes for a given temperature level ($500^0$C) on the burning front to pass successive thermocouples. The results indicate that the burning front spreads essentially at a constant rate.

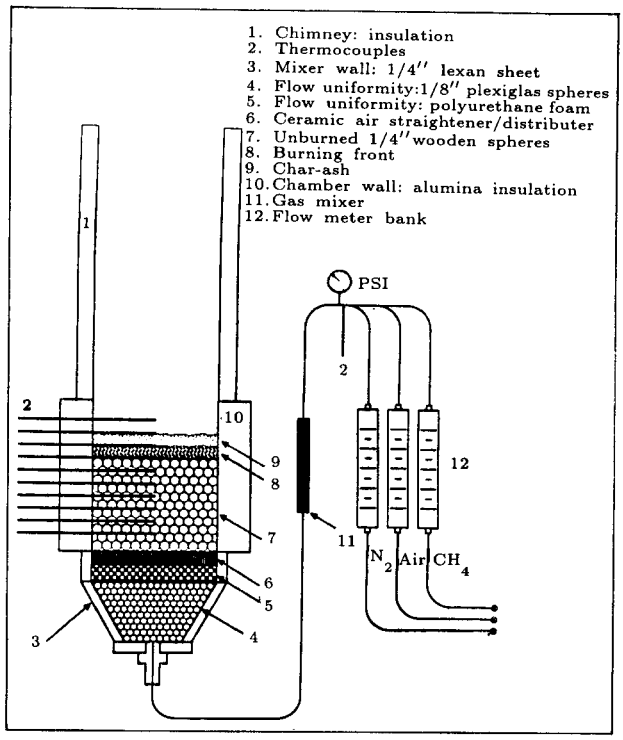


**Figure 7.** Schematic of the experimental apparatus.

Air is supplied from below in the opposite direction to the front propagation and its velocity is calculated from the measured volumetric flow rate into the bed and its cross-sectional area. To study the effect of gas flow rate on the combustion characteristics of the bed, the air flow rate is varied between $4 \times 10^{-5}$ ($m^3/s$) and $1.6 \times 10^{-3}$($m^3/s$). The lower and upper values

**Table 3.** Base-Case Properties

| | | Gas Properties | Process Parameters | Solid Properties |
|---|---|---|---|---|
| $c_p$ | kJ/kg K | 1.05 | – | 2.81 |
| $k$ | W/m K | $26.3 \times 10^{-3}$ | – | 0.15 |
| $\rho$ | kg/m$^3$ | 1.16 | – | 663 |
| $D_{mg}$ | m$^2$/s | $2.1 \times 10^{-5}$ | – | – |
| $\Delta i_c$ | MJ/kg Fuel | – | 14 | – |
| $n_o$ | kg $O_2$/kg Fuel | – | 1.25 | – |
| $F$ | – | – | 0.68 | – |
| $d$ | m | – | $6.4 \times 10^{-3}$ | – |
| $E$ | kJ/mol | – | 163 | – |
| $A$ | $s^{-1}$ | – | $5.67 \times 10^9$ | – |

set the flammability limits in the experiment. It has been observed experimentally that air flow rates above $8 \times 10^{-4}$(m$^3$/s) result in incipient fluidization of the top layers, which have lower density (due to the solid consumption) than the unburned solid.

## Results

The thermophysical properties that are used in the analytical and numerical calculations are shown in Table 3. The heat capacity and thermal conductivity for air (at 300K) and wood are given by Incropera and DeWitt [77] and assumed to be independent of temperature. The binary mass diffusion coefficient (oxygen-nitrogen) and its dependence on temperature is given by Reid et al. [78]. The amount of oxygen required for the stoichiometric burning of wood, $n_o$, is 1.25 (kg $O_2$ /kg fuel) [79] and the heating value for wood, $\Delta i_c$, is taken to be 14 (MJ/kg fuel) as reported by Summitt and Sliker [80].

Figure 8 illustrates a typical combustion wave structure obtained numerically. The spatial variation of temperature, oxygen, unburned solid and reaction rate is shown in the preheat zone, the reaction zone and downstream of the reaction wave. The results are obtained for the adiabatic reverse combustion, assuming local thermal equilibrium between the phases. The

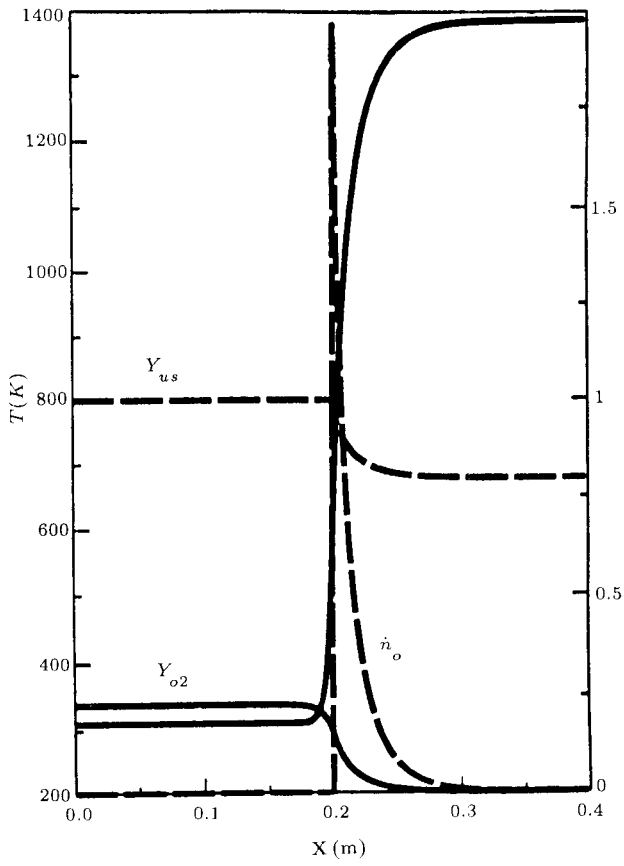


**Figure 8.** Combustion wave structure.

mass concentration of oxygen essentially goes to zero over the width of the reaction zone and some solid fuel will remain unreacted. The degree of solid consumption depends on the initial air flow rate and oxygen supply.

The burning velocity is essentially controlled by the balance between the degree of heat generation in the reaction zone and transport of this heat to the unburned solid fuel. Thus, radiation becomes an important factor in controlling the rate at which the burning front spreads to the unreacted zone. The final temperature and the degree of consumption of solid fuel (or the apparent equivalence ratio) depend on the propagation velocity, which is not known a priori. At low air flow rates, the reaction is oxygen limited and the apparent equivalence ratio is only a fraction of that for the stoichiometric. Increasing the air flow rate results in higher burning velocities, accompanied by higher temperatures and a shift in the equivalence ratio toward stoichiometric. Beyond a critical flow rate (stoichiometric burning), the solid will be totally consumed and excess oxygen will remain at the end of the reaction zone (fuel limited). Figures 9 and 10 show our numerical calculations for the variation of the combustion wave velocity and the maximum temperatures with respect to the inlet air velocity, in comparison with the experimental and analytical results. In Figure 9, the point where the burning velocity crosses the stoichiometric line corresponds to the total consumption of both the oxygen and solid fuel.

## COMBUSTIBLE POROUS MEDIUM: SOLID-SOLID REACTIONS

The propagation of a reaction front in an ignited powder mixture of reactants A and B is possible if a sufficient fraction of the heat generated in this exothermic reaction (combustion) can flow downstream of the front. The heat and mass transfer through the powder (and within the individual particles) is significantly altered

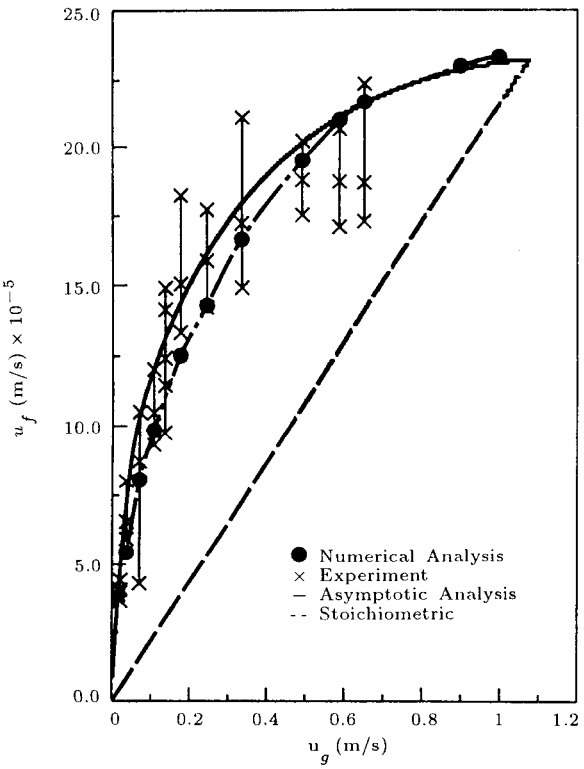


**Figure 9.** Variation of the burning front propagation rate with the inlet air velocity.

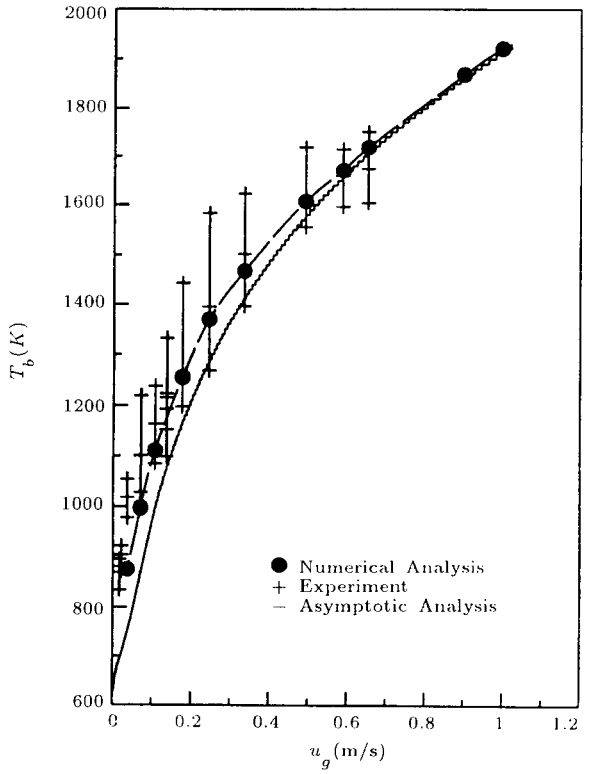


**Figure 10.** Variation of the peak burning temperature with the inlet velocity.

**Table 4.** Examples of Systems Used in Combustion Synthesis

| Reaction | Crystal | $\Delta i_c$ (kJ/kg) | $T_{AB,m}$(°C) | $T_{A,m}$(°C) | $T_{B,m}$(°C) | $T_{ad}$(°C) |
|---|---|---|---|---|---|---|
| $Ti_\ell + C_s \rightarrow TiC_s$ | Gry met, Cub | -3076 | $3140 \pm 90$ | $1660 \pm 10$ | 3652 subl | 2937 |
| $Ti_\ell + 2B_s \rightarrow TiB_{2s}$ | Hex | -4663 | 2900 | $1660 \pm 10$ | 2300 | 2917 |
| $3Ti_\ell + B_4C_s \rightarrow 2TiB_{2s} + TiC_s$ | - | - | - | $1660 \pm 10$ | - | - |
| $Si_\ell + C_s \rightarrow SiC_s$ | Blk. Cub ($\beta$) | -1629 | 2700 subl | 1410 | 3652 subl | 1527 |
| $Si_\ell + C_s \rightarrow SiC_s$ | Blk, Hex ($\alpha$) | -1566 | 2700 subl | 1410 | 3652 subl | 1527 |
| $Zr_\ell + C_s \rightarrow ZrC_s$ | Gry met, Cub | -1967 | 3540 | 1852 | 3652 subl | |
| $Hf_\ell + C_s \rightarrow HfC_s$ | - | -1321 | ca 3890 | 2227 | 3652 subl | 3627 |
| $Nb_\ell + C_s \rightarrow NbC_s$ | Blk Gry, Cub | -1325 | 3500 | 2468 | 3652 subl | |
| $4B_\ell + C_s \rightarrow B_4C_s$ | Blk, Rhbdr | -1288 | 2350 | 2300 | 3652 subl | 727 |
| $3Cr_\ell + 2C_s \rightarrow Cr_3C_{2s}$ | Gry, Rhomb | -449 | 1980 | 1857 | 3652 subl | |

The properties are taken from CRC Handbook of Chemistry and Physics (1986-1987) and from Handbook of Thermodynamics Tables and Charts (1976).

if melting occurs and especially if the liquid phase moves due to capillarity (assuming that the Bond number $B_o = g\rho_\ell d^2/\sigma$ is small enough, i.e., the gravity effect is negligible compared to capillarity). In many binary systems, the melting point of one or both reactants is below the adiabatic stoichiometric reaction temperature, and it is expected that the transport (and reaction) around the combustion front will be influenced by the presence of the liquid phase and will be significantly different than that associated with transport through the solid phase only. This, in general, results in enhanced diffusion and, therefore, both the front speed and the extent of reaction completion (especially for volume-averaged nonstoichiometric mixtures and when particles of A and B are not in direct contact) increase due to the formation and movement of the liquid phase. The grain structure of the product is also influenced by this liquid.

We consider the reaction

$$A_\ell + B_s \longrightarrow AB_s. \tag{79}$$

Table 4 gives examples of the binary systems A and B used in the combustion synthesis of product AB [81, 82], where $\Delta i_c$ is the heat of reaction; $T_{AB,m}$ is the melting point of stoichiometric AB; $T_{A,m}$ and $T_{B,m}$ are the melting points of pure A and B species; and $T_{ad}$ is the adiabatic stoichiometric reaction temperature. For example, as shown in Table 4, $T_{A,m}$ is less than $T_{ad}$ for the Ti and C system and for the Si and C system.

The description of transport and reaction through porous media (when the formation of a liquid phase is included) is by a set of local volume-averaged governing equations where local thermal and concentration equilibria are assumed between the liquid and solid phases and no allowance is made for the motion of the liquid [83, 84, 85]. The rationale for these simplifications has been the search for the gross rather than the detailed behavior of the combustion front. On the other hand, for binary systems that undergo phase change, the experimental studies have unveiled many interesting features, which can only be explained in light of the liquid formation and motion [81, 86].

In the descriptions of Margolis [84, 87]

when the species A has a melting point below the adiabatic combustion temperature, a liquid film of this species will form around the B particles. The amount of liquid and the mass transfer within it, and between the liquid and the solid phases, are not yet addressed. Because of the lack of a direct inclusion of the liquid and its distribution, the role of the liquid formation is generally only lumped into an empirical parameter combining the degree of reaction completion and the latent heat of fusion [83, 84]. On the other hand in the liquid phase sintering literature (where the entire specimen is assumed to be at a uniform temperature), the formation of the liquid phase and its motion (including the motion of the solid particles totally surrounded by the molten) is more directly addressed [88, 89].

The present state of the knowledge on combustion synthesis is nearly completely summarized in the proceeding of the international conference held in 1988 and in the summary of a recent workshop [90]. The mathematical treatments (including stability) are reviewed by Bayliss and Matkowsky [91], Margolis et al. [92], Armstrong and Koszykowski [93], and Varma et al. [94]. The experimental and physical aspects are discussed by Hardt and Holsinger [95], Mullins and Riley [96], Anselmi-Tamburini and Munir [97], Trambukis and Munir [98], and Deevi [81].

A pore-level examination of the reacting powders (for impermeable spherical particles) reveals that a liquid phase is formed and that initially (up to the time where a critical local liquid volume is reached) this liquid is held as rings at the particle-particle contact points (where the reactions occur). At higher liquid volumes, the liquid phase becomes continuous (at least over several particles) and is mobile. In general, there is also a two-phase state (i.e., the mushy region) separating the liquid and the solid phases. This is also realized by examining the phase diagram of the binary systems and by noting that when the adiabatic combustion

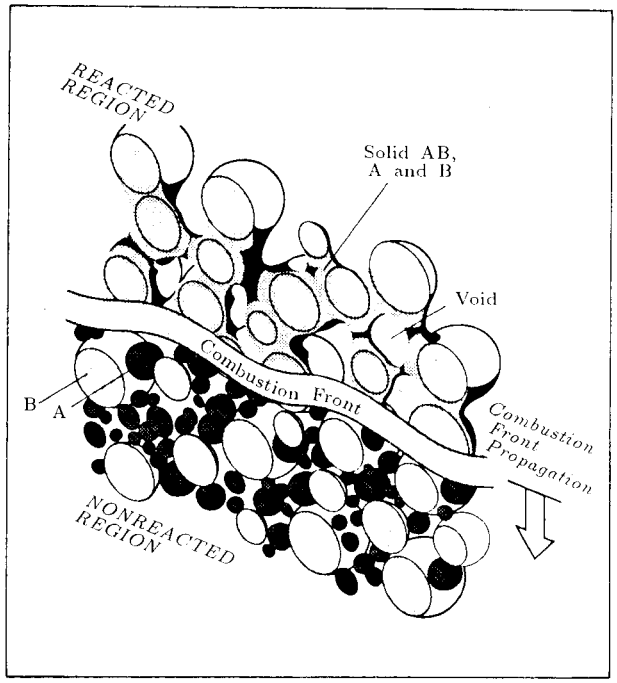


**Figure 11.** A rendering of the reacted and unreacted regions adjacent to the combustion front.

temperature lies between the melting point of species A (lower melting point) and species B, the product of A and B can be in the two-phase state for parts of the concentration spectrum. An example is the carbon-titanium system. Note that after a sufficient amount of time is elapsed and for stoichiometric mixtures where particles of A and B are in direct contact through at least one interface, no unreacted A and B will remain. Figure 11 gives a rendering of the reacted and unreacted regions adjacent to the combustion front. The volume-averaged nonstoichiometric and diluted mixtures will have some special features. We point out the particle-level reaction as being controlled by both diffusion and liquid motion and that except for a particular plane in each particle, this reaction is always nonstoichiometric. Therefore, the liquid and two-phase zone formation and motion is rather complicated and in powder reactions, an approach similar to that taken for continuum (mostly slabs) solidification and melting [93, 97, 99] must be taken. The molecular mass diffusivity of liquids is larger

than that of solids and a favorable distribution of the liquid phase can significantly increase the rate of completion of the reaction and the propagation speed of the combustion front. With the formation of liquid (and for small enough particles), the single-temperature wave propagation may occur; while for no melting (as is for large particles), the two-temperature wave propagation (the second one marking the completion of the reaction) may occur [82]. The spread of the liquid may also result in a structural anisotropy of the final product.

These features can only be unveiled by a pore-level examination of the transport, reaction and phase change. In practice, the pore-level simulations are too elaborate to use and, therefore, local volume-averaged descriptions are used. The local volume-averaged governing equations that apply to combustion synthesis must include some of the above-mentioned, pore-level features in order to result in accurate predictions of the local concentration (i.e., the transient degree of completion of the reaction). As will be shown in the proposed research, this would require a separate local treatment of the liquid and the solid phases (i.e., imposition of local nonequilibrium). The inclusion of pore-level features requires prescription of some coefficients coupling the transport equations for each phase. An estimation of these coupling coefficients is generally found by the analysis of the pore-level phenomena (i.e., a direct simulation at the pore-level). Presently, this direct simulation and the appropriate local volume-averaged descriptions are not available. It should be mentioned that for the verification of the direct simulations and the predictions of the local volume-averaged equations, experimental results are needed that specifically address the parameters appearing in the analysis. Therefore, because of the required simplifications/assumptions made in any analysis, critical experimental verifications must be coupled into the investigation. So far this detailed investigation has not been applied to the combustion synthesis.

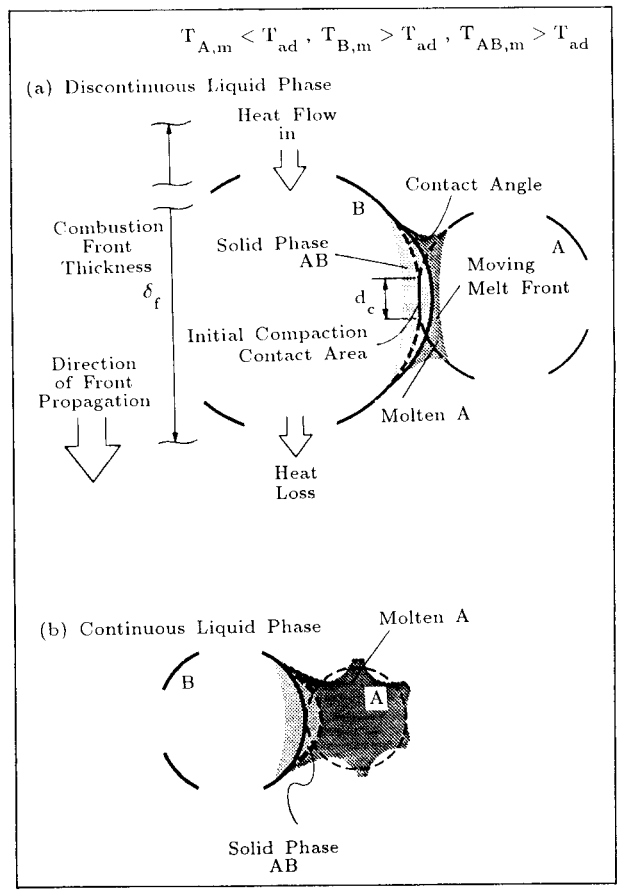


**Figure 12.** The reaction and melting front penetration at a particle-particle contact area. (a) The liquid is discontinuous and appears as rings around the contact area. (b) The liquid from the adjacent pores connect and a continuous liquid phase is formed.

## Analysis of Solid-Solid Reaction

### *Mass Transfer*

Assume that the green specimen is made of monosize particles of species A with diameter $d_A$ and monosize species B with diameter $d_B$ with an initial compaction assigned by the initial contact area given by the contact diameter $d_{c_{AA}}$, $d_{c_{AB}}$, and $d_{c_{BB}}$ Figures 12 and 13 give a rendering of the arrangement of the particles. The symbols are defined in the nomenclature section. A statistical arrangement is also possible by an ensemble averaging over many realizations of

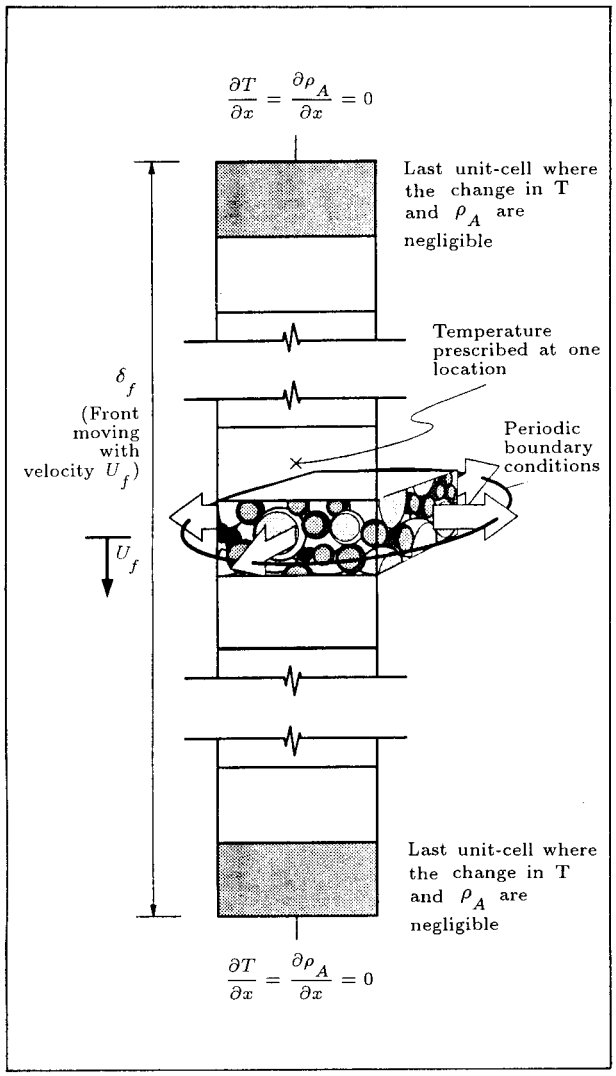


**Figure 13.** The unit cell used for the direct simulation of the propagation. Several such unit cells are included upstream and downstream of the front and the simultaneous solution to the transport in these unit cells is sought.

some arrangements.

The species A and B diffuse through their contact area and react at the reaction rate given by a phenomenological chemical kinetic relation of the form [85]

$$\dot{n}_A = \rho_A K_o(T) exp(-E/RT)\cdot \qquad (80)$$

This exothermic reaction generates heat at a rate of $\dot{n}_A \Delta i_c$ (W/m$^3$) and this heat will partly result in an increase in the local sensible heats and will also be consumed as the latent heat. The mass diffusion of A and B continues and becomes enhanced due to the increase in the local temperature and also due to the high molecular mass diffusivity through the liquid phase. Depending on the particle sizes, a capillary motion may occur and can further enhance the mass transfer and, hence, the reaction rate. The dependence of the molecular mass diffusivity on the temperature is generally given through phenomenological models such as [99]

$$D_{m,A-AB} = (D_{m,A-AB})_o \, exp(-\Delta i_{a,A-AB}/RT)\cdot \qquad (81)$$

Note that we have been discussing impermeable spherical particles and so far have not mentioned porous spherical particles such as porous carbon made of an agglomeration of soot particles [81]. In such cases, the molten can penetrate through these pores (due to capillarity) and the rate of penetration into these porous particles is much larger than that due to molecular diffusion (even at elevated temperatures). In particles of species A or B, diffusion, phase change and reaction occur as determined by the initial contact area, particle arrangement and the thermo-physico chemical properties. These phenomena will be determined by solving the conservation equations along with the appropriate constitutive relations and by allowing for the property variations. The lateral periodic boundary conditions can be justifiably applied. However, longitudinally the combustion front covers many particles and there is no symmetry. Therefore, in both the upstream and downstream (with respect to the front propagation direction), many unit cells will be included in the direct simulation.

### *Heat Transfer*

For each particle, heat flows in from the neighboring upstream particles. When there is a sig-

nificant difference between the thermal diffusivities of particles A and B, a significant amount of heat can also flow laterally into the particle. The heat is also generated due to reaction, and finally it flows out to the downstream particles (and if $\alpha_A/\alpha_B$ is far from unity, also laterally). The mass and heat diffusion and reaction and heat generation results in temperatures above the melting temperature of species A, causing a phase change. As was pointed out, the phase change of the binary systems includes the mushy regime where a two-phase mixture also exists. The existing treatments also include the continuum model in which the transition from the solid to liquid phase through the mushy zone is through a continuous change in the solid fraction.

The coupled heat and mass transfer equations for the unit cell can be solved by tracking the interfaces in each particle. The unit cells are connected through their common boundaries, and the entire combustion front will be simulated by seeking the steady solution (by making the control volumes move with the eigenvalue front speed, as done in the computation of premixed gaseous combustion).

### *Liquid Meniscus*

The liquid and mush formed can move due to the forces of the volume expansion during the formation of these phases (and in the solidification zone downstream of the front, the liquid that was moved there by capillarity will undergo a volume decrease) and the capillarity. The opposing forces are the static surface forces (at the three-phase contact line, the force balance leads to the static contact angle) and, when the liquid is in motion, the viscous force. Determination of the quasi-steady meniscus contour in the downstream liquid-phase regime when no mushy zone present, is rather straightforward [4]. The inclusion of the mushy zone and the dynamic forces add complications that have not yet been addressed. One can include the mushy zone as a pseudo-liquid phase but with properties different from the liquid. This will allow us to use the contact angle (either static or modified-advancing or receding). This in turn will allow for the estimation of the trajectory of the moving contact line (i.e., the line between the three solid, liquid, and gaseous phases) and the gradual connection of the menisci of the neighboring rings (i.e., start of the liquid continuity). The static Young-Laplace formulation for the meniscus is generally not applicable to fast transient problems, such as the one considered here. However, the trends predicted by the modified static formulation (i.e., by inclusion of the dynamic contact angle and the dependence of the surface tension on the concentration, etc.) have been found to agree with the experimental results [100].

### *Thermodynamics*

Figure 14(a) is a binary phase diagram reproduced from German [88] that shows that the species A has a melting point below the adiabatic mixture temperature $T_{ad}$, a characteristic favorable for reactive liquid phase sintering. Note that for particles made of pure A and pure B species, the entire concentration spectrum is realized as the two particles A and B come in contact at elevated temperatures. The two-phase regimes (i.e., $\ell + s$), as well as the liquid and solid regimes, are present in the phase diagram. In principle, the thermal penetration front through a particle of species A is followed by a concentration front (notwithstanding that the mass diffusivity increases with temperature as given by Hardt and Phung [99]). Then at a position in the particle with $T \simeq T_{A,m}$ and with the concentration of species A higher than $C_{\ell 1}$, a liquid phase exists. For $C_{\ell 2} < C_A < C_{\ell 1}$ and $T \simeq T_{A,m}$, a two-phase region is first encountered before arriving at a solid phase region, which is followed by another two-phase region. As is clear, this can be a fairly complicated phase distribution in a particle A undergoing

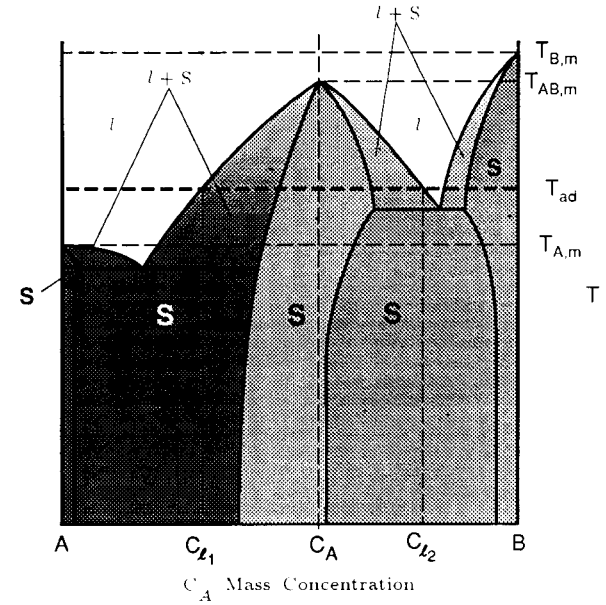


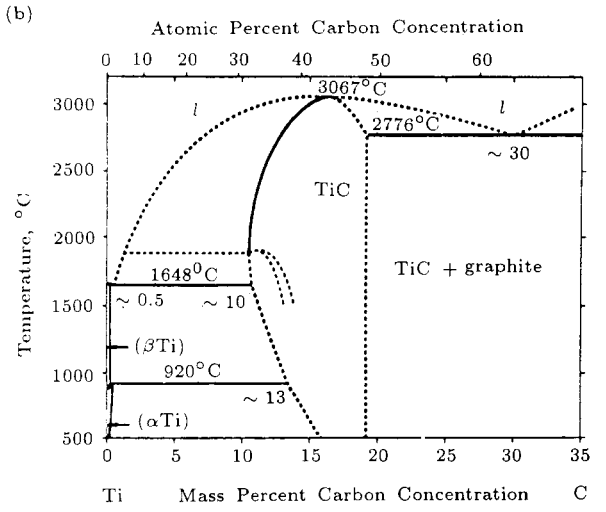


**Figure 14**. (a) A rendering of the phase diagram for a binary system with $T_{A,m} < T_{ad}$. The diagram is suggested by German [88] for systems favorable for reactive liquid phase sintering. (b) The phase diagram for Ti-C binary system from Massalski [101].

reaction with the neighboring particle B. Note that these are equilibrium phase characteristics and, in general, for fast phase change conditions such as that considered here, the equilibrium phase diagram may not be realized.

Figure 14(b) is the phase diagram for the Ti-C system [101]. The high carbon concentration portion is not shown. This is an example of a very commonly used system [81, 102, 96, 103, 82]. The encountering of various phases during reaction is evident.

## NOMENCLATURE

| | |
|---|---|
| A | reactant A, or pre-exponential factor ($s^{-1}$), or area ($m^2$) |
| AB | product |
| B | reactant B |
| $B_o$ | Bond number ($= g\rho_\ell d^2/\sigma$) |
| $c$ | specific heat (J/kg-K) |
| $C$ | average interparticle spacing |
| $C_A$ | mass fraction of species A |
| $d$ | diameter (m) |
| $d_c$ | contact diameter (m) |
| D | mass diffusivity ($m^2/s$) |
| $\mathbf{D}^d$ | dispersion tensor |
| $E$ | activation energy for reaction (J/kg) |
| F | exchange factor |
| $g$ | gravity constant ($m/s^2$) |
| $h$ | interfacial coefficient |
| $h_D$ | diffusion controlled reaction ($kg/m^3s$) |
| $\Delta i_c$ | heat of formation (J/kg) |
| $k$ | thermal conductivity (W/m-K) |
| $K_o$ | reaction constant |
| $\boldsymbol{K}$ | thermal conductivity tensor |
| $K$ | kinetically controlled reaction ($kg/m^3s$) |
| $Le$ | Lewis number |
| $\dot{n}$ | reaction rate |
| $Pe$ | Peclect number |
| $R$ | gas constant (J/kg-K) |
| $Sh$ | Sherwood number |
| $t$ | time (s) |
| $T$ | temperature (K) |
| $T_{A,m}$ | melting temperature of pure A (K) |
| $T_{AB,m}$ | melting temperature of product AB (K) |
| $T_{ad}$ | adiabatic temperature (K) |
| $T_{B,m}$ | melting temperature of pure B (K) |

$u$ velocity (m/s)
$V$ volume ($m^3$)
$x$ spatial coordinate (m)
$Y$ mass fraction

***Greek symbols***

$\alpha$ thermal diffusivity ($m^2/s$)
$\delta$ combustion front thickness (m)
$\epsilon$ porosity
$\lambda$ wavelength
$\rho$ density ($kg/m^3$)
$\sigma$ surface tension (N/m), or Stefan-Boltzman constant ($W/m^2K^4$)
$\Phi$ equivalence ratio

***Superscripts***

$d$ dispersion
$\ell$ liquid
$g$ gas
$s$ solid

***Subscripts***

A species A
$a$ ash
B species B
$b$ downstream
$D$ Darcy
$e$ effective
$f$ front or fluid
$g$ gas
$gp$ gaseous products
$i$ initial
$I$ inert
$\ell$ liquid
$m$ mass or melting point
$o$ reference, or oxygen
$s$ solid
$u$ upstream
$us$ unburned solid
$x$ x-coordinate

***Others***

$\langle\ \rangle$ local volume averaging symbol

## REFERENCES


1. Nozad, I., Carbonell, R.G. and Whitaker, S. "Heat conduction in multi-phase systems, I: Theory and experiment for two-phase systems," *Chem. Engng. Sci.* **40**, pp 843-855 (1985).
2. Prat, M. "On the boundary conditions at the macroscopic level," *Trans. Porous Media*, **4**, pp 259-280 (1989).
3. Sahraoui, M. and Kaviany, M. "Slip and no-slip temperature boundary conditions at interface of porous plain media: Conduction," *Int. J. Heat Mass Transfer*, **36**, pp 1019-1033 (1992).
4. Kaviany, M. *Principles of Heat Transfer in Porous Media*, Springer-Verlag Publishers, New York (1991).
5. Koch, D.L. and Brady, J. "Dispersion in fixed beds," *J. Fluid Mech.*, **154**, pp 399-427 (1985).
6. Koch, D.L., Cox, R.G., Brenner, H. and Brady, J."The effect of order on dispersion in porous media," *J. Fluid Mech.*, **200**, pp 173-188 (1989).
7. Sahraoui, M. and Kaviany, M. "Slip and no-slip temperature boundary conditions at interface of porous plain media: convection," *Int. J. Heat Mass Transfer*, in print (1994).
8. Vortmeyer, D. "Radiation in packed solids," *Proc., 6th Int. Heat Transfer Conference*, **6**, pp 325-539 (1978).
9. Singh, B.P. and Kaviany, M. "Independent theory versus direct simulation of radiation heat transfer in packed beds," *Int. J. Heat Mass Transfer*, **34**, pp 2869-2881 (1991).
10. Carbonell, R.G. and Whitaker, S. "Heat

and mass transfer in porous media," In *Fundamentals of Transport in Porous Media*, Bear and Corpaerglu, Eds., Martinus Nijhoff Publishers, pp 123-198 (1984).

11. Wako, N. and Kaguei, S. *Heat and Mass Transfer in Packed Beds*, Gordon and Breach Science Publishers (1982).
12. Siegel, R. and Howell, J.R. *Thermal Radiation Heat Transfer*, 2nd edn., McGraw-Hill, New York (1981).
13. Ozisik, M.N. *Radiative Transfer and Interaction with Conduction and Convection*, Werbel and Peck, New York (1985).
14. Hottel, H.C., Sarofim, A.F., Dalzell, W.H. and Vasalos, I.A. "Optical properties of coatings, effect of pigment concentration," *AIAA J.*, **9**, pp 1895-1898 (1971).
15. Brewster, M.Q. "Radiative Heat Transfer in Fluidized Bed Combustors," *ASME*, 83-WA/HT-82 (1982).
16. Yamada, Y., Cartigny, J.D. and Tein, C.L. "Radiative transfer with dependent scattering by particles: Part 2-Experimental investigation," *J. Heat Transfer*, **108**, pp 614-618 (1986).
17. Drolen, B.L. and Tein, C.L. "Independent and dependent scattering in packed spheres systems," *J. Thermophysics Heat Transfer*, **1**, pp 63-68 (1987).
18. Ishimaru, A. and Kuga, Y. "Attenuation constant of a coherent field in a dense distribution of particles," *J. Optics Soc. of Amer.*, **72**, pp 1317-1320 (1982).
19. Cartigny, J.D., Yamada, Y. and Tein, C.L. "Radiative heat transfer with dependent scattering by particles: Part 1--Theoretical investigation," *J. Heat Transfer*, **108**, pp 608-613 (1986).
20. Kumar, S. and Tein, C.L. "Dependent scattering and absorption of radiation by small particles," *Proc., 24th National Heat Transfer Conference*, ASME HTD, **72**, pp 1-7 (1987).
21. Yang, Y.S., Howell, J.R. and Klein, D.E. "Radiative heat transfer through a randomly packed bed of spheres by the Monte Carlo method", *J. Heat Transfer*, **105**, pp 325-332 (1963).
22. Kudo, K., Yang, W.J., Tanaguchi, H. and Hayasaka, H. "Radiative heat transfer in packed spheres by Monte Carlo method," *Proc., Heat Transfer in High Tech. and Power Eng.*, pp 529-540 (1987).
23. Tein, C.L. and Drolen, B.L. "Thermal radiation in particulate media with dependent and independent scattering," *Ann. Rev. of Num. Fluid Mech. Heat Tran.*, **1**, pp 1-32 (1987).
24. Chen, J.C. and Churchill, S.W. "Radiation heat transfer in packed beds," *AIChE J.*, **9**, pp 35-41 (1963).
25. Tong, T.W., Yang, Q.S. and Tein, C.L., "Radiative heat transfer in fibrous insulations, 1. Theoretical study," *ASME* paper no. 81-HT-42 (1981).
26. Tong, T.W., Sathe, S.B. and Peck R.E. "Improving the performance of porous radiant burners through the use of submicron size fibers," In *Heat Transfer in Radiation, Combustion and Fires*, ASME HTD, **106** (1989).
27. Singh, B. and Kaviany, M. "Modelling dependent scattering in radiation heat transfer in packed beds," *Int. J. Heat Mass Transfer*, **35**, pp 1397-1405 (1992).
28. Singh, B.P. and Kaviany, M. "Effect of solid conductivity on radiative heat transfer in packed beds," *Int. J. Heat Mass Transfer*, submitted (1994).
29. Jodrey, W.S. and Tory, E.M. "Simulation of random packing of spheres," *Simulation*, **Jan.**, pp 1-12 (1979).

30. Kotani, Y. and Takeno, T. "An experimental study on stability and combustion characteristics of an excess enthalpy," *19th Symp. (Intl.) Combust.*, The Combustion Institute, pp 1503-1509 (1982).
31. Echigo, R., Kurusu, M., Ichimiya, K. and Yoshizawa, Y. "Combustion augmentation of externally low calorific gases," *Proc., ASME/JSME Thermal Eng. Joint Conference*, **IV**, pp 99-103 (1983).
32. Chen, Y.K., Matthews, R.D. and Howell, J.R. "The effect of radiation on the structure of premixed flame within a highly porous inert medium," *ASME HTD*, **81**, pp 35-42 (1987).
33. Yoshizawa, Y., Sasaki, K. and Echigo, R. "Analytical study of the structure of radiation controlled flame," *Int. J. Heat Mass Transfer*, **31** (2), pp 311-319 (1988).
34. Khinkis, M.J., Kunc, W. and Xoing, T-Y. "Experimental evaluation of a high-efficiency surface combustor-heater concept with low pollutant emissions," *Int. Symp. on Combustion in Industrial Furnaces and Boilers*, American Flame Research Committee, Short Hills, New Jersey (1989).
35. Sathe, S.B., Peck, R.E. and Tong, T.W. "A numerical analysis of heat transfer and combustion in porous radiant burners," *Int. J. Heat Mass Transfer*, **33** (6), pp 1331-1338 (1990).
36. Echigo, R. "Radiative enhanced/ controlled phenomena of heat and mass transfer in porous media," *Proc., Third ASME/JSME Thermal Eng. Joint Conf.*, **4**, pp xxi-xxxii (1991).
37. Hsu, P.-F., Howell, J.R. and Mathews, R.D. "A numerical investigation of premixed combustion within porous inert media," *Proc., Third ASME/JSME Thermal Eng. Joint Conf.*, **4**, pp 225-231 (1991).
38. Babkin, V.S., Korzhavin, A.A. and Bunev, V.A., "Propagation of premixed gaseous explosion flames in porous media," *Combust. Flame*, **87**, pp 182-190 (1991).
39. McIntosh, A.C. and Prothero, A. "A model of large heat transfer surface combustion with radiant heat emission," *Combust. Flame*, **83**, pp 111-126 (1991).
40. Yoshizawa, Y. "Study of the limit temperature of adiabatic combustion systems," *JSME Int. J. Series II*, **32**, pp 227-233 (1991).
41. Sathe, S.B., Peck, R.E. and Tong, T.W. "Flame stabilization and multimode heat transfer in inert porous media: A numerical study," *Combust. Sci. and Tech.*, **70**, pp 93-109 (1990).
42. Bernstein, M.E. and Churchill, S.W. "Multiple stationary states and $NO_x$ production for turbulent flames in refractory tubes," *6th Symp. (Intl.) Comb.*, Combustion Institute, p 1737 (1977).
43. Pfefferle, L.D. "Stability, ignition and pollutant formation characteristics of combustion in thermally stabilized plug-flow burners," Ph.D. thesis, University of Pennsylvania, Phil., PA (1984).
44. Taylor, G.I., "Dispersion of soluble matter in solvent flowing slowly through a tube," *Proc. Roy. Soc.*, (London), A219, pp 186-203 (1953).
45. Glassman, I., *Combustion*, 2nd edn. Academic Press (1987).
46. O'Sullivan, J.B. and Khinkis, M.J. "Developments in ultra-low-emission natural gas combustion," presented at Vancouver Industrial Gas, **90** (1990).
47. Sathe, S.B., Kulkarni, M.R., Peck R.E. and Tong, T.W. "An experimental study of combustion and heat transfer in porous radiant burners", presented at the fall meeting of the Western States Section of the Combustion Institute, Livermore, CA (1989).
48. Egolfopoulos, F.N. and Law, C.K. "Chain mechanisms in the overall reaction orders in laminar flame propagation," *Combust.*

*Flame*, **80**, pp 7-16 (1990).

49. Williams, F.A. *Combustion Theory*, Addison Wesley (1988).

50. Ryan, D., Carbonell, R.G. and Whitaker, S. "Effective diffusivities for catalyst pellets under reactive conditions," *Chem. Engng. Sci.*, **35**, pp 10-16 (1980).

51. Pfefferle, L.D. and Pfefferle, W.C. "Catalysis in combustion," *Catal. Rev.-Sci. Eng.*, **29**, pp 219-267 (1987).

52. Griffin, T.A. and Pfefferle, L.D. "Gas phase and catalytic ignition of methane and ethane in air over platinum" *AIChE J.*, **36**, pp 861-870 (1990).

53. Marteney, P.J. and Kesten, A.S. "Kinetics of surface reactions in catalytic combustion," *18th Symp. (Intl.) Comb.*, pp 1899-1908 (1981).

54. Harrison, B.K. and Ernst, W.R. "Catalytic combustion in cylindrical channels: A homogeneous-heterogeneous model" *Combust. Sci. Tech.*, **19**, pp 31-38 (1978).

55. Bruno, C., Walsh, P.M., Santavicca, D.A., Sinha, N., Yaw, Y. and Bracco, F.V. "Catalytic combustion of propane/air mixture on platinum," *Combust. Sci. Tech.*, **31**, pp 43-74 (1983).

56. Fakher, A. and Buckius, R.O. "Transient catalytic combustion on a flat plate," *Combust. Flame*, **52**, pp 169-184 (1983).

57. Ohlemiller, J.T. and Lucca, D.A. "An experimental comparison of forward and reverse smolder propagation in permeable fuel beds," *Combust. Flame*, **54**, pp 131-147 (1983).

58. Ohlemiller, T.J. "Modeling of smoldering combustion propagation," *Prog. Energy Combust. Sci.* **11**, pp 277-310 (1985).

59. Palmer, K.N. "Smouldering combustion in dusts and fibrous materials," *Combust. Flame*, **1**, pp 129-154 (1957).

60. Moussa, N.A., Toong, T.Y. and Garris, C.A. "Mechanism of smoldering of cellulosic materials," *16th Symp. (Intl.) Comb.*, Combustion Institute, p 1447 (1977).

61. Summerfield, M., Ohlemiiler, T.J. and Sandusky, H.W. "A thermophysical mathematical model of steady-draw smoking and predictions of overall cigarette behavior," *Combust. Flame*, **33**, pp 263-279 (1978).

62. Dosanjh, S.S., Pagni, P.J. and Fernandez-Pello, A.C. "Forced cocurrent smoldering combustion," *Combust. Flame*, **68**, pp 131-142 (1987).

63. Ohlemiller, T.J. *Smoldering Combustion Hazards of Thermal Insulation Materials*, National Bureau of Standards, Washington, DC. (1981).

64. Ohlemiller, T.J. "Smoldering combustion propagation through a permeable horizontal fuel layer," *Combust. Flame*, **81**, pp 341-353 (1990).

65. Ohlemiller, T.J. *Forced Smolder Propagation and the Transition to Flaming in Cellulosic Insulation*, National Bureau of Standards, Washington, DC (1985).

66. Ohlemiller, T.J. "Forced smolder propagation and the transition to flaming in cellulosic insulation," *Combust. Flame*, **81**, pp 354-365 (1990).

67. Rogers, F.E. and Ohlemiller, T.J. "Cellulosic insulation materials I. Overall degradation kinetics and reaction heats," *Combust. Sci. Tech.*, **24**, pp 129-137 (1990).

68. Rogers, F.E. and Ohlemiller, T.J. "Smolder characteristics of flexible polyurethane foams," *J. Fire Flammability*, **11**, pp 32-44 (1980).

69. Ohlemiller, T.J., Bellan, J., and Rogers, F. "A model of smoldering combustion applied to flexible polyurethane foams," *Combust. Flame*, **36**, pp 197-215 (1979).

70. Robinovich, O.S. and Gurevich, F.G. "Low-temperature technological combustion of porous systems with forced filteration of a gas reagent," *Int. J. Heat Mass Transfer*, **29**, pp 241-255 (1986).

71. Kashiwagi, T. and Nambu, H. "Global kinetic constants for thermal oxidative degradation of a cellulosic paper" *Combust. Flame*, **88**, pp 345-368 (1992).

72. Roberts, A.F. "A review of kinetics data for the pyrolysis of wood and related substances," *Combust. Flame*, **14**, pp 261-272 (1970).

73. Shafizadeh, F. "The chemistry of pyrolysis and combustion," In *The Chemistry of Solid Wood*, R. Rowell, Ed., ACS, Washington, DC, pp 489-529 (1984).

74. Parker, W.J. "Prediction of the heat release rate of wood," Ph.D. dissertation, The George Washington University (1988).

75. Golombok, M., Jariwala, H. and Shirvill, L.C. "Gas-solid heat exchange in a fibrous metallic material measured by a heat regenerator technique," *Int. J. Heat Mass Transfer*, **33**, pp 243-252 (1990).

76. Patankar, S.V. *Numerical Heat Transfer and Fluid Flow*, Hemisphere Publishing Corp., NY (1980).

77. Incropera, F.P. and DeWitt, D.P. *Introduction to Heat Transfer*, 2nd Edn., John Wiley & Sons, Inc. (1985).

78. Reid, R.C., Prausnitz, J.M., and Poling, B.E. *The Properties of Gases and Liquids*, 4th Edn., McGraw-Hill Book Company (1987).

79. Tillman, D.A., Rossi, A.J. and Kitto, W.D., 1981, *Wood Combustion: Principles, Processes, and Economics*, Academic Press (1981).

80. Summitt, R., and Sliker, A. *Handbook of Materials Science*, CRC Press, Inc. (1980).

81. Deevi, S.C. "Structure of the combustion wave in the combustion synthesis of titanium carbide" *J. Mater. Sci.*, **26**, pp 2662-2670 (1991).

82. Munir, Z.A. "Synthesis of high temperature materials by self-propagating combustion methods," *Ceramic Bull.*, **67**, pp 342-349 (1988).

83. Merzhanov, A, G. "Self-propagating high-temperature synthesis: twenty years of search and finding," In *Combustion and Plasma Synthesis of High-Temperature Materials*, Z.A. Munir and J.B. Holt, Eds., VCH Publishers, pp 1-53 (1990).

84. Margolis, S.B. "An asymptotic theory of condensed two-phase flame propagation," *SIAM J. Appl. Math.*, **43**, pp 351-369 (1983).

85. Merzhanov, A.G. and Averson, A.E. "The present state of the thermal ignition theory: An invited review," *Combust. Flame*, **16**, pp 89-124 (1971).

86. Rabin, B.H. Bose, A. and German, R.M. "Combustion synthesis of nickel aluminides," In *Combustion and Plasma Synthesis of High-Temperature Materials*, Z.A. Munir and J.B. Holt, Eds., VCH Publishers, pp 114-121 (1990).

87. Margolis, S.B. "An asymptotic theory of heterogeneous condensed combustion," *Combust. Sci. and Tech.*, **43**, pp 197-215 (1985).

88. German, R.M. *Liquid Phase Sintering*, Plenum Press (1985).

89. Somiya, S. and Moriyoshi, Y. *Sintering Key Papers*, Elsevier Science Publishers (1990).

90. Grosshandler, W.A., Ed. *Research Needs in Direct Combustion Synthesis*; summary of a National Science Foundation workshop (February 21-22, 1990).

91. Bayliss, A. and Matkowsky, B.J. "Modeling and numerical computation of a non-steady SHS process," In *Combustion and*

*Plasma Synthesis of High-Temperature Materials*, Z.A. Munir and J.B. Holt, Eds, VCH Publishers, pp 61-72 (1990).

92. Margolis, S.B. Matkowsky, B.J., and Booty, M.R. "New models of quasiperiodic burning combustion synthesis," In *Combustion and Plasma Synthesis of High-Temperature Materials*, Z.A. Munir and J.B. Holt, Eds, VCH Publishers, pp 73-82 (1990).
93. Armstrong, R. and Koszykowski, M., "Combustion theory of sandwiches of alloyable materials," In *Combustion and Plasma Synthesis of High-Temperature Materials*, Z.A. Munir and J.B. Holt, Eds, VCH Publishers, pp 88-99 (1990).
94. Varma, A., Cao, G. and Morbidelli, M. "Self-propagating solid-solid noncatalytic reaction in finite pellets," *AIChE J.*, **36**, pp 1032-1038 (1990).
95. Hardt, A.P. and Holsinger, R.W. "Propagation of gasless reactions in solids, II. Experimental study of exothermic intermetallic reaction rates," *Combust. Flame*, **21**, pp 91-97 (1973).
96. Mullins, M.E. and Riley, E., "The effect of carbon morphology on the combustion synthesis of titanium carbide," *J. Mater. Res.*, **4**, pp 408-411 (1989).
97. Anselm-Tamburini, U. and Munir, Z.A. "Observation on the combustion reaction between thin foils of Ni and Al," In *Combustion and Plasma Synthesis of High-Temperature Materials*, Z.A. Munir and J.B. Holt, Eds, VCH Publishers, pp 100-105 (1990).
98. Trambukis, J. and Munir, Z.A. "Effects of particle dispersion on the mechanism of combustion synthesis of titanium silicide," *J. Amer. Ceramic Soc.*, **73**, pp 1240-1245 (1990).
99. Hardt, A.P. and Phung, P.V. "Propagation of gasless reactions in solids, I. Analytical study of exothermic intermetallic reaction rates," *Combust. Flame*, **21**, pp 77-89 (1973).
100. Tao, Y.-X. and Kaviany, M., "Simultaneous heat and mass transfer from a two-dimensional partially liquid covered surface," *J. Heat Transfer*, **113**, pp 875-882 (1991).
101. Massalski, T., Ed. *Binary Alloy Phase Diagram*, **1**, ASM (1986).
102. Advani, A.H., Thadhani, N.N., Grebe, H.A., Heaps, R., Coffin, C. and Kottke, T. "Dynamic modeling of self propagating high temperature synthesis of titanium carbide ceramics," *Script. Metal. Mater.*, **25**, pp 1447-1452 (1991).
103. Adachi, S., Wada, T., Mihara, T., Miyamoto, Y., Koizumi, M. and Yamada, O. "Fabrication of titanium carbide ceramics by high-temperature self-combustion sintering of titanium powder and carbon fiber," *J. Amer. Ceramic Soc.*, **72**, pp 805-809 (1989).